iScience

CellPress

Article

Virus- and Interferon Alpha-Induced Transcriptomes of Cells from the Microbat *Myotis daubentonii*

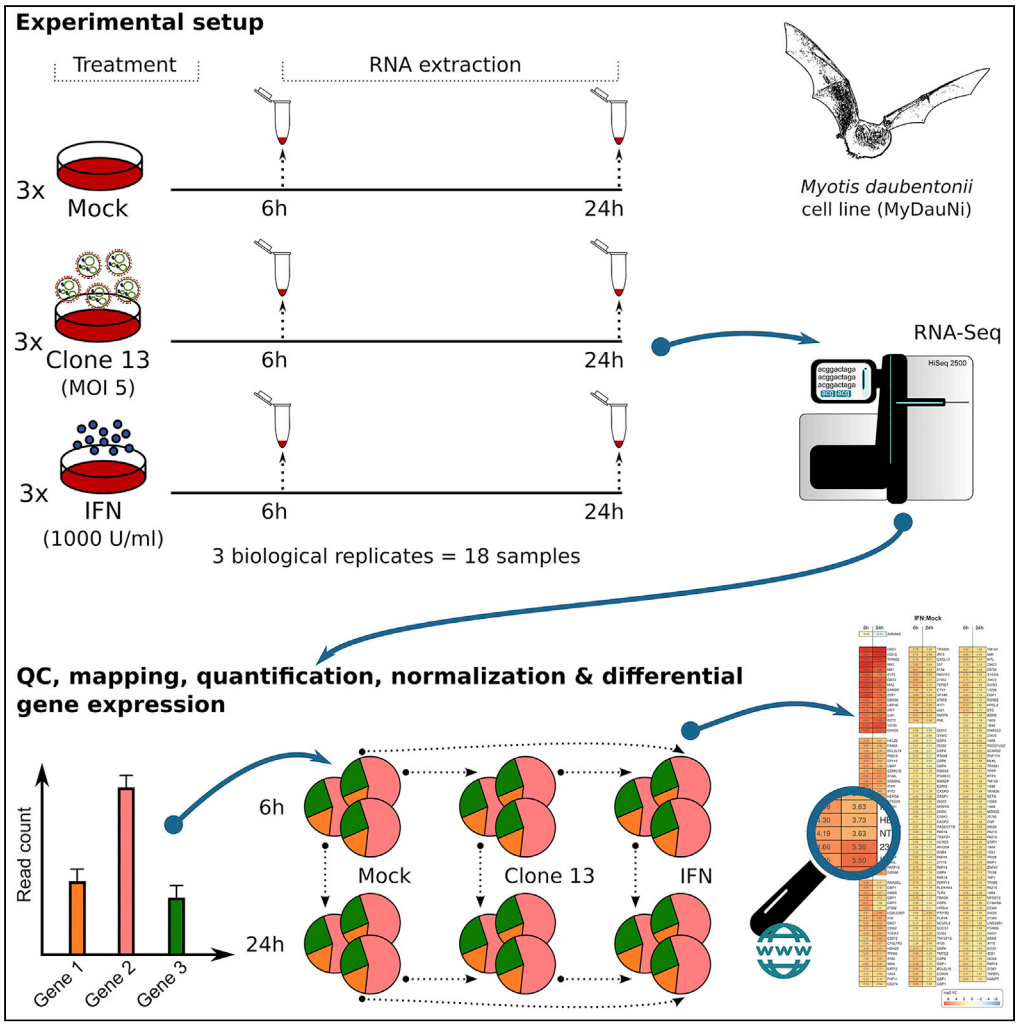

Martin Hölzer, Andreas Schoen, Julia Wulle, Marcel A. Müller, Christian Drosten, Manja Marz, Friedemann Weber

manja@uni-jena.de (M.M.)
friedemann.weber@vetmed.uni-giessen.de (F.W.)

HIGHLIGHTS

Virus- and IFN-responsive transcriptomes of the microbat *Myotis daubentonii*

CCL4, IFNL3, CH25H, STEAP4 are IFNB-like genes triggered by virus only

Microbats encode more paralogs of BST2 (tetherin) than any other mammal

Clear differences between the IFN systems of microbats and megabats

DATA AND CODE AVAILABILITY

GSE121301

Hölzer et al., iScience *19*, 647–661
September 27, 2019
https://doi.org/10.1016/j.isci.2019.08.016

iScience

CellPress

Article

Virus- and Interferon Alpha-Induced Transcriptomes of Cells from the Microbat *Myotis daubentonii*

Martin Hölzer,[1,2,8] Andreas Schoen,[3,4,5,8] Julia Wulle,[3,4,5] Marcel A. Müller,[5,6,7] Christian Drosten,[5,6] Manja Marz,[1,2,*] and Friedemann Weber[3,4,5,9,*]

SUMMARY

Antiviral interferons (IFN-alpha/beta) are possibly responsible for the high tolerance of bats to zoonotic viruses. Previous studies focused on the IFN system of megabats (suborder *Yinpterochiroptera*). We present statistically robust RNA sequencing (RNA-seq) data on transcriptomes of cells from the "microbat" *Myotis daubentonii* (suborder *Yangochiroptera*) responding at 6 and 24 h to either an IFN-inducing virus or treatment with IFN. Our data reveal genes triggered only by virus, either in both humans and *Myotis* (CCL4, IFNL3, CH25H), or exclusively in *Myotis* (STEAP4). *Myotis* cells also express a series of conserved IFN-stimulated genes (ISGs) and an unusually high paralog number of the antiviral ISG BST2 (tetherin) but lack several ISGs that were described for megabats (EMC2, FILIP1, IL17RC, OTOGL, SLC24A1). Also, in contrast to megabats, we detected neither different IFN-alpha subtypes nor an unusually high baseline expression of IFNs. Thus, *Yangochiroptera* microbats, represented by *Myotis*, may possess an IFN system with distinctive features.

INTRODUCTION

Bats are major reservoirs for viral zoonotic pathogens. Virus infections that are acute and highly aggressive in humans can be persistent and avirulent in bats (Calisher et al., 2006). An important contributor of virus tolerance by bats is thought to be the antiviral type I interferon (IFN-α/β) system (Dobson, 2005). Indeed, in some bats the IFN system has peculiar features and is under strong positive selection (De La Cruz-Rivera et al., 2018; Pavlovich et al., 2018; Yan, 2015; Zhang et al., 2013; Zhou et al., 2016). Bats may thus possess a fortified IFN system that suppresses viruses down to levels of persistence (Dobson, 2005; Pavlovich et al., 2018; Wynne and Wang, 2013; Zhang et al., 2013).

Type I IFNs are a group of cytokines that encompass several subtypes, such as IFN-β, IFN-α 1 to 13, and some others (Garcin et al., 2013). Type III IFNs (IFN-λ 1, 2, 3) are similar, but unlike the systemic type I IFNs they act locally on epithelial cells (Hamming et al., 2010). IFN induction occurs by cellular sensing of viral RNA structures, resulting in the activation of IFN transcription factors, such as IRF3. The once-secreted IFNs bind to their receptor, activate the transcription factors STAT1/2 via the JAK kinases, and drive the expression of multiple IFN-stimulated genes (ISGs) with antiviral and immunomodulatory activity (Schoggins, 2014).

Prototypical ISGs respond only to IFN signaling. However, there are ISGs additionally or even exclusively activated after virus sensing. Thus, the IFN response encompasses virus-response genes (IRF dependent), IFN-specific ISGs (STAT dependent), and universal ISGs (responding to both infection and IFNs) (Schmid et al., 2010).

Bats (order *Chiroptera*) are classified into the suborders *Yinpterochiroptera* (Syn. *Pteropodiformes*) and *Yangochiroptera* (Syn. *Vespertilioniformes*) (Teeling et al., 2018). Members of both suborders are infected by a wide range of virus species (Calisher et al., 2006). However, despite some progress, the contribution of the IFN response to their special ability to host viruses is not yet clarified. For *Yinpterochiroptera* such as *Pteropus alecto*, *vampyrus* or *Rousettus aegyptiacus* (all family *Pteropodidae*, or "megabats"), several studies had measured the global transcriptional response of cells to infection with, e.g., Ebola, Marburg, Nipah, or Hendra virus (Hölzer et al., 2016; Kuzmin et al., 2017; Wynne et al., 2014) or to the IFN-inducing Newcastle Disease virus (NDV) (Glennon et al., 2015). By contrast, for the more diverse bat suborder

[1]RNA Bioinformatics and High-Throughput Analysis, Friedrich Schiller University Jena, Jena, Germany

[2]European Virus Bioinformatics Center, Jena, Germany

[3]Institute for Virology, FB10-Veterinary Medicine, Justus-Liebig University, Giessen, Germany

[4]Institute for Virology, Philipps University Marburg, Marburg, Germany

[5]German Centre for Infection Research (DZIF), partner sites Marburg, Giessen, and Charité Berlin, Germany

[6]Institute of Virology, Charité-Universitätsmedizin Berlin, corporate member of Freie Universität Berlin, Humboldt-Universität zu Berlin, and Berlin Institute of Health, Berlin, Germany

[7]Martsinovsky Institute of Medical Parasitology, Tropical and Vector Borne Diseases, Sechenov University, Moscow, Russia

[8]These authors contributed equally

[9]Lead contact

*Correspondence: manja@uni-jena.de (M.M.), friedemann.weber@vetmed.uni-giessen.de (F.W.)

https://doi.org/10.1016/j.isci.2019.08.016

Yangochiroptera (generically termed "microbats") there are just two virus-induced cell transcriptomes available (Gerrard et al., 2017; Wu et al., 2013). However, the full virus response capability of bats remains uncharted because almost all cell response studies bar one (Glennon et al., 2015) with megabats and all studies with microbats employed wild-type viruses, which are weak IFN inducers. With respect to the response to IFN itself, there are expression profiles of cells from the megabat *P. alecto* (De La Cruz-Rivera et al., 2018; Zhang et al., 2017), and Shaw et al. recently conducted a pan-species comparison of IFN-stimulated cell transcriptomes, which included the megabat *P. vampyrus* and the *Yangochiroptera* microbat (family *Vespertilionidae*) *Myotis lucifugus* (Shaw et al., 2017).

Thus, previous studies on virus-induced or IFN-stimulated transcriptional profiles of cells overwhelmingly focused on megabats (family *Pteropodidae*) of the suborder *Yinpterochiroptera*. This suborder contains 7 bat families, whereas the *Yangochiroptera*, having separated around 60 million years ago, contain 14 families (Teeling et al., 2018). *Yangochiroptera* species host SARS-like coronaviruses (Drexler et al., 2011), rhabdoviruses and flaviviruses (Calisher et al., 2006), paramyxoviruses (Drexler et al., 2012), and bunyaviruses such as Crimean-Congo hemorrhagic fever-like virus (Muller et al., 2016), Hantavirus (Weiss et al., 2012), or Rift Valley fever virus (Calisher et al., 2006; Oelofsen and Van der Ryst, 1999). Nonetheless, for *Yangochiroptera* microbats there are (1) no studies on the transcriptomal cell responses to an IFN-inducing virus and (2) only one study on the IFN-stimulated gene expression profile (Shaw et al., 2017), which, however, focused on conserved ISGs. Moreover, to our knowledge a side-by-side, global comparison of early and late transcriptomes of cells in response to either virus or IFN is not available for any organism.

To fill these gaps, we devised a study for the *Yangochiroptera* microbat *Myotis daubentonii* (family *Vespertilionidae*). *M. daubentonii* is a carrier of lyssaviruses prevailing from Europe to Japan (McElhinney et al., 2018). On the phylogenetical tree, it is maximally separated from the previously studied *Pteropodidae* megabats (Teeling et al., 2018). We stimulated *M. daubentonii* cells either with a strong IFN inducer virus or with type I IFN and measured global transcription at two different time points. Our results reveal several unique features like novel virus-response genes and an elevated number of paralogs of the antiviral ISG BST2. Unlike reported for megabats (Pavlovich et al., 2018; Zhou et al., 2016) we could not detect different IFN-alpha subtypes or unusually high base levels of IFNs. Thus, besides exhibiting conserved antiviral responses and ISGs, several traits of the *Yangochiroptera* microbats are unique and not even observed for megabats.

RESULTS AND DISCUSSION

Outline of the Experiments to Measure Transcriptomes

The aim of our study was to obtain the full picture of the antiviral type I IFN response of the *Yangochiroptera* microbat representative *M. daubentonii*, using a kidney cell line (MyDauNi/2c) described previously (Fuchs et al., 2017; Muller et al., 2012). IFNs have anti-proliferative activity, which is the reason why many cell lines have lost their ability to induce IFN and/or to respond to IFN over their passaging history (Hess et al., 2012). MyDauNi/2c cells, however, exhibited the typical phosphorylation of STAT1 in response to exogenously added pan-species IFN-α B/D (Figure S1A). Moreover, STAT1 phosphorylation was downmodulated by Ruxolitinib, an established inhibitor of JAK1/2-mediated IFN signaling (Stewart et al., 2014). STAT1 phosphorylation and Ruxolitinib effect were comparable with the IFN-competent human A549 (Kuri et al., 2010; Weber et al., 2015) and the *R. aegytiacus* megabat cell line Ro6E-J (Fuchs et al., 2017) that we used in parallel. These results demonstrate the capacity of the MyDauNi/2c cells to respond to IFN.

To elucidate the overall antiviral potency and the unimpeded ability to produce IFN in response to infection, we employed a mutant of Rift Valley fever virus that has its IFN suppressor NSs replaced by the *Renilla* luciferase gene (RVFVΔNSs::Renilla) (Kuri et al., 2010). RVFVΔNSs::Renilla is a strong inducer of type I IFNs, is sensitive to the antiviral action of IFNs, and able to infect cells from a wide range of vertebrates (Kuri et al., 2010). The built-in *Renilla* luciferase facilitates rapid and quantitative measurements of viral replication. Also, the *M. daubentonii* MyDauNi/2c cells could be infected with our reporter virus, permitting replication levels similar as in human A549 lung cell line or the fetal *R. aegytiacus* line Ro6E-J (Jordan et al., 2009) (Figure S1B). Moreover, treatment with the IFN signaling inhibitor Ruxolitinib increased RVFVΔNSs::Renilla replication, whereas IFN-α suppressed it. Although the cell lines are from different organs, these results, taken together, demonstrate that our immortalized *Yangochiroptera*/*Vespertilionidae* cell line MyDauNi/2c possesses a fully functional IFN system that is comparable with the one of human and megabat cell lines.

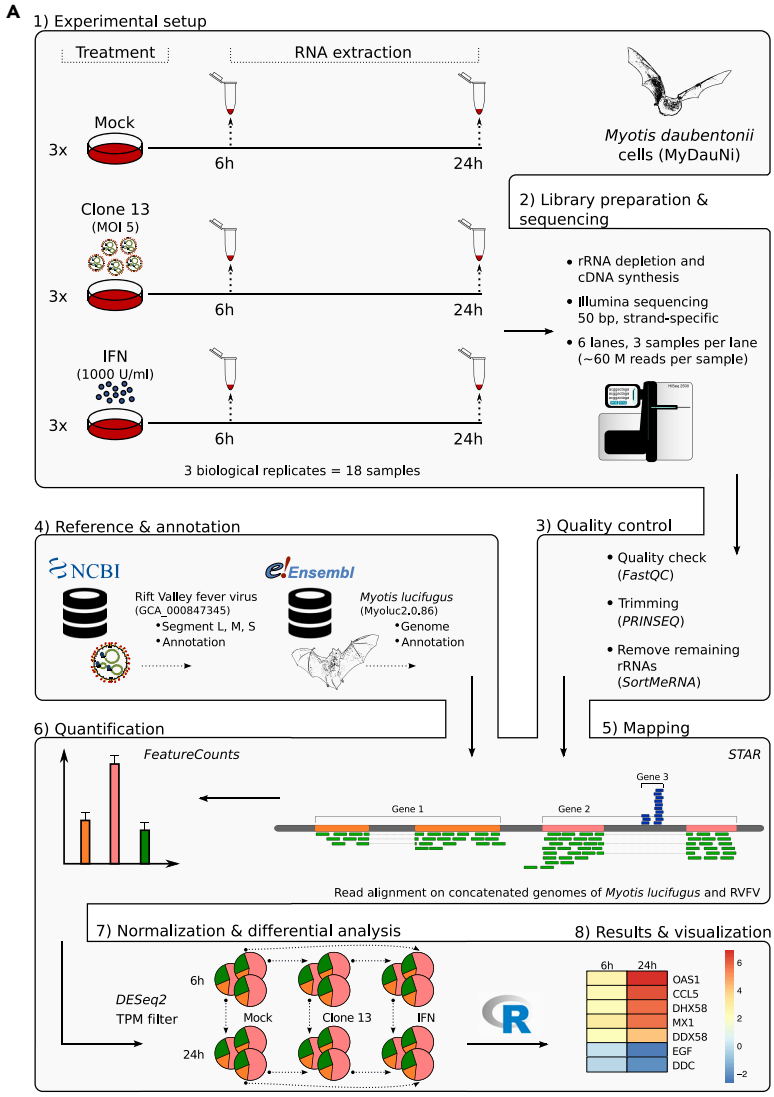
A
1) Experimental setup
Treatment
RNA extraction
Mock
3x
6h
24h
Clone 13
(MOI 5)
IFN
(1000 U/ml)
Myotis daubentonii
cells (MyDauNi)
3 biological replicates = 18 samples
2) Library preparation & sequencing
• rRNA depletion and cDNA synthesis
• Illumina sequencing 50 bp, strand-specific
• 6 lanes, 3 samples per lane (~60 M reads per sample)
4) Reference & annotation
NCBI
Ensembl
Rift Valley fever virus
(GCA_000847345)
•Segment L, M, S
•Annotation
Myotis lucifugus
(Myoluc2.0.86)
•Genome
•Annotation
3) Quality control
• Quality check (FastQC)
• Trimming (PRINSEQ)
• Remove remaining rRNAs (SortMeRNA)
6) Quantification
FeatureCounts
5) Mapping
STAR
Gene 1
Gene 2
Gene 3
Read alignment on concatenated genomes of Myotis lucifugus and RVFV
7) Normalization & differential analysis
DESeq2
TPM filter
8) Results & visualization
OAS1
CCL5
DHX58
MX1
DDX58
EGF
DDC

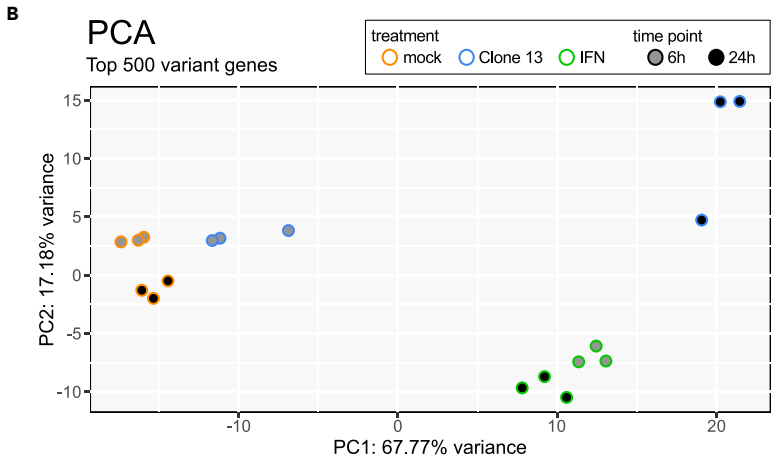
B
PCA
Top 500 variant genes
treatment
mock
Clone 13
IFN
time point
6h
24h
PC2: 17.18% variance
PC1: 67.77% variance

Figure 1. Experiments and Analyses to measure *M. daubentonii* Transcriptomes in Response to Virus and IFN
(A) Workflow.
(B) Principal component analyses. The biological replicates of the transcriptomes of uninfected (mock), Clone 13-infected, and IFN-treated cells, sampled at two different time points, were analyzed and visualized by PCAGO (see text).

Figure 1A gives an overview of the experimental setup. The MyDauNi/2c cells were either mock treated, infected with a strong IFN inducer (RVFV NSs mutant Clone 13) (Billecocq et al., 2004), or treated with 1,000 U/ml IFN-α. Total cell RNAs were isolated at 6 and 24 h post infection, and rRNA-depleted cDNA libraries were sequenced with 60–70 million strand-specific single-end reads per sample (Table S1). Of note, all experiments were performed in three independent, biological replicates.

Around 70% of the quality-checked and trimmed reads could be uniquely mapped to the reference genome of the related *M. lucifugus* (Table S2), using appropriate tools (Dobin and Gingeras, 2015; Kopylova et al., 2012; Schmieder and Edwards, 2011). Based on pairwise comparisons of the mean values of the three replicates, protein-encoding genes that were induced or repressed by an absolute log2 fold change (FC) $\geq$ 2 and with an adjusted p $\leq$ 0.05 (DESeq2 (v1.16.1) [Love et al., 2014]) were defined as significantly responding to either Clone 13 infection or IFN. To test whether biological replicates cluster together, we performed various principal component analyses (PCA) using our PCAGO web service (https://doi.org/10.1101/433078). In general, and visualized by the PCA based on the top 500 variant genes (Figures 1B and S2A), we found the biological replicates to cluster together. The PCA revealed that the transcriptomes of the 6-h post Clone 13 infection samples are closest to the mock samples and that the IFN-stimulated profiles of both time points are highly similar. The highest variance in the data (PC1 with 67,77%) can be explained by the large expression differences between the mock and Clone 13 6-h samples compared with the Clone 13 and IFN-stimulated 24-h samples. At 24 h, the Clone 13-infected cells show an expression pattern that is clearly distinguishable from all other conditions. One of the Clone 13 24-h replicates clustered somewhat apart from the other two replicates (see Figure 1B), but the difference between these accounts for only 3.3% (PC2; Figure S2B) of the whole variation in the gene expression data when directly compared with the mock 24-h samples. A 2D- and a 3D-PCA-movie, visualizing the overall stable clustering and how the principal components change by adding more and more less-variant genes to the transformation, can be found in the online supplement (Videos S1 and S2). CLARK classification (Ounit et al., 2015) and Krona visualization (Ondov et al., 2011) revealed ~1% of the reads with high similarity to the RVFV reference genome in this specific sample, compared with 3%–4% in the other two replicates (Figure S3). In addition to our reference-based analyses, we have created a comprehensive *de novo* transcriptome assembly for *M. daubentonii* by combining (Fu et al., 2012) the output of various suitable assembly tools (Bankevich et al., 2012; Grabherr et al., 2011; Liu et al., 2016; Xie et al., 2014) according to the results of Hölzer and Marz (Hölzer and Marz, 2019).

Virus-Responsive Genes

At 6 h post infection with the IFN inducer virus Clone 13, 21 genes were upregulated (Figures 2A and 2B). Among these were prototypical, IRF3-driven genes (IFNB1, CCL5, CXCL10, IFIT1 to 3, OAS1, and OASL), and others reported to be expressed by infected cells (DDX58, DDX60, DHX58, IFIH1, IFI44, ISG15) (Balogh et al., 2014; Doganay et al., 2017; Glennon et al., 2015; Grandvaux et al., 2002; McWhirter et al., 2004; Puthia et al., 2016; Schmid et al., 2010). By contrast, upregulated genes such as IRF7, MX1, MX2, OAS3, SAMD9, and USP18 are prototypical ISGs (Rusinova et al., 2013; Shaw et al., 2017) that most likely are activated by the Clone 13-induced IFN in the supernatant (see later discussion). Altogether the upregulated genes are commanding biological processes of the immediate-early innate response to viruses, as shown by GO term enrichment using the Piano package (Varemo et al., 2013) (Figure S4A, upper panel).

At 24 h post infection, 246 genes were upregulated and 13 genes were downregulated. All the genes from the 6-h time point are included in the 24-h-upregulated genes (see Figures 2A and 2B). Comparisons with the pan-species database of IFN-triggered transcriptomes (Shaw et al., 2017) identified conserved additional ISGs (besides the ones mentioned for the 6-h time point) such as, e.g., ADAR, BST2, various GBPs, HERC6, IFITM 2 and 3, IRF9, PARP12, PML, RSAD2, TRIM22, SOCS1, STAT1, STAT2, or ZBP1. SAMHD1, by contrast, was recently described as being IRF3 dependent in human, monkey, and porcine cells (Yang et al., 2016). Among the late virus responders were also more unusual genes such as CSF2 or NEURL3. Both are weakly IFN stimulated in *Rattus norvegicus* but not in any other mammalian species (Shaw et al., 2017). In *M. daubentonii*, CSF2 is exclusively virus inducible (see below) and NEURL3 is strongly virus as well as (weakly) IFN inducible.

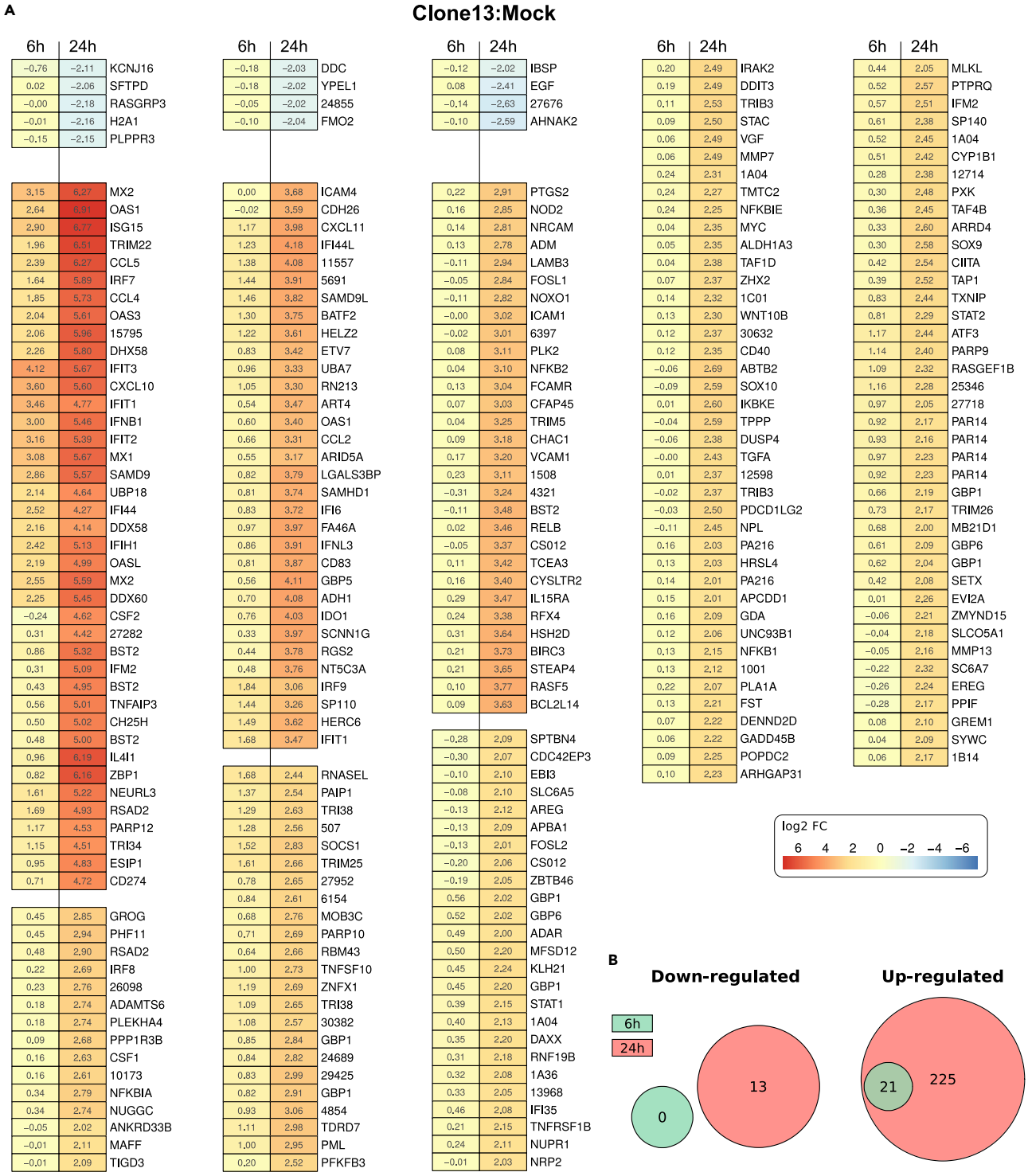

Figure 2. *Myotis daubentonii* Genes Differentially Regulated in Response to Clone 13 Infection

(A) Heatmap of log2-fold changes in infected cells as compared with mock infected cells. The displayed genes were filtered by an absolute log2-fold change of 2 and an adjusted p value < 0.05. Genes that are similarly regulated at 6 and 24 h post infection are clustered together. Data are averages from three biological replicates. Genes missing a gene name and a function in the current Ensembl annotation of *M. lucifugus* were listed by their unique and abbreviated ID numbers: e.g., "ENSMLUG00000015795" was shortened to "15795."

(B) Venn diagrams showing the numbers of significantly regulated mRNAs at the two time points of infection.

The genes upregulated at this later time point were functionally more diversified than the 6-h ones, as they promote adaptive immunity, apoptosis, and also RNA polymerase II activity, besides the innate immune response (Figure S4A, lower panel). The genes downregulated at 24 h post infection were mostly involved in carbohydrate metabolism and protein transport.

All significantly up- or downregulated genes can be investigated with our Interactive Gene Observer search tool https://www.rna.uni-jena.de/supplements/mda/report.html which was was modified from the output of the Reporting Tools package (Huntley et al., 2013). Full gene tables and expression statistics for the individual biological replicates and all pairwise comparisons can be found in the electronic supplement, Figure S5. Coverage of viral genome is documented in Figure S6.

IFN-Responsive Genes

When cells were treated for 6 h with IFN, 195 genes were strongly upregulated (i.e., substantially more than after 6 h of Clone 13 infection). No gene was downregulated (Figures 3A and 3B). The IFN-regulated genes encompassed prototypical (OAS1, ISG15, Mx1, IFIT3, BST2, DHX58) but also less known ISGs (BCL2L14, RNF213, ESIP1).

At 24 h, the number of upregulated genes was decreased to 106, of which 1 gene (PLA1A) was actually unique for this late time point. Moreover, just 1 gene (AHNAK2) is significantly downregulated at 24 h. Thus, *M. daubentonii* cells are capable of rapidly responding to IFN, and at the 24-h time point almost half of the stimulated genes were back to base levels. This transient character of the type I IFN response is in agreement with recent studies on cells from megabat (*P. alecto*) (De La Cruz-Rivera et al., 2018), man (Jilg et al., 2014), and mouse (Mostafavi et al., 2016).

For the IFN-stimulated transcriptomes, predominant biological processes both at 6 and 24 h post infection encompassed antigen processing and presentation, antiviral defense, immune response, and NF-kB regulation (Figure S4B). Additionally, at 6 h there are indications of both up- and downregulation of intracellular and transmembrane transport, and at 24 h oxidoreductase activity is mostly downregulated.

Genes Uniquely Regulated by Virus Infection

To our knowledge, a kinetic and side-by-side comparison of virus-driven versus IFN-driven host cell transcriptomes was not reported for any mammalian species so far. Therefore, beyond the bat-specific aspects this study was initiated for, we took advantage of our database to filter out genes that are uniquely regulated by either treatment. To address this issue, we compared gene expression at the 6- and 24-h time points of Clone 13 infection and IFN treatment with each other. Overall, running the two transcriptomes next to each other showed once more that at 6 h Clone 13 infection stimulated less genes (denominated as being "downregulated") than 6-h IFN treatment (Figures 4A and 4B). We could identify some genes that are upregulated exclusively by Clone 13, most prominently the prototypical, IRF3-driven virus-response gene IFNB1. When restricting ourselves to genes that were not at all regulated by IFN but upregulated by a log2 of more than 3 by virus (i.e., stricter than the log2-fold change of 2 filter we had set for the heatmaps), a similar virus-only response behavior was exhibited by other cytokines such as, e.g., CCL2, CCL4, IFNL3 (IFN-λ3), and CSF2, and also by more untypical genes such as CH25H, ICAM1, and STEAP4. Figure 4C shows RNA-seq data as expression box plots to illustrate the exclusive virus-response behavior in *M. daubentonii* cells.

Not all these genes are known as pure virus responders. Therefore, we verified our findings by RT-qPCR for the strongest early virus responders (IFNB1, CCL4, IFNL3, CH25H, STEAP4) and compared with the human system. Although being a late responder, CH25H (cholesterol 25-hydroxylase) is included because it is a powerful, broad-spectrum virus inhibitor. Human A549 and MyDauNi cells were infected with Clone 13, treated with IFN, or left untreated, and samples were taken 6 and 24 h later. Moreover, to exclude any potential cross talk by virus-triggered IFN, we kept in parallel cells under the JAK/STAT signaling inhibitor Ruxolitinib. In both the human and the *Myotis* cells, Ruxolitinib expectedly inhibited STAT1 phosphorylation and upregulation of the prototypical IFN-dependent ISG Mx1 (Figure S7). The RT-qPCR data shown in Figure 5 demonstrate that IFNB1, CCL4, IFNL3, and CH25A are exclusively virus induced with no stimulation whatsoever by IFN. (Of note, a downmodulation of IFNB1 at 24 h post infection was detected by RT-qPCR but not by the less sensitive NGS [see Figure 2].) This was true for both the human and the *M. daubentonii* cells, indicating a conserved behavior. STEAP4 (six transmembrane epithelial antigen of prostate), by contrast, was identified as a virus-only response gene in *M. daubentonii* cells but unresponsive to both IFN and Clone 13 in human cells.

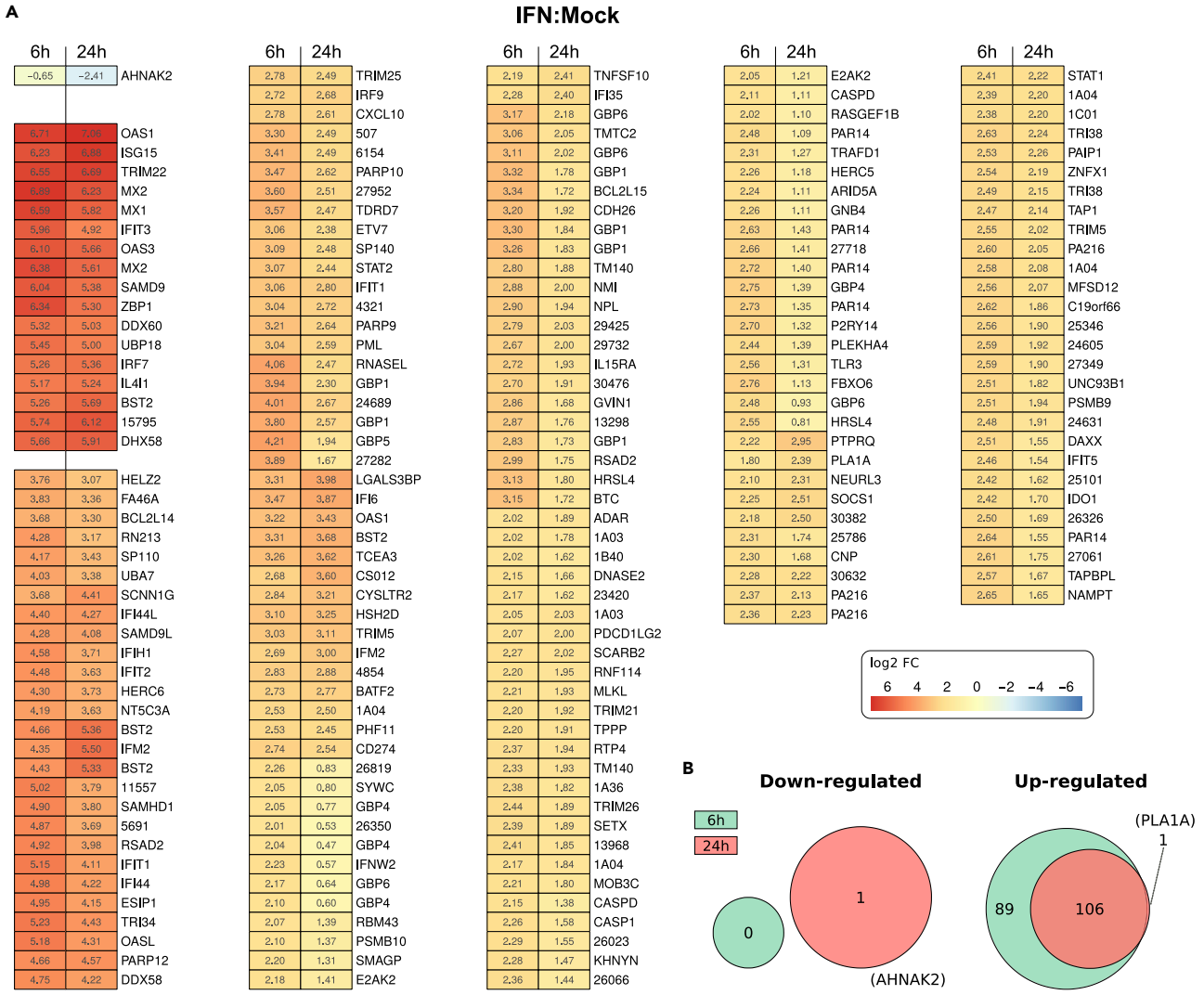

Figure 3. *Myotis daubentonii* Genes Differentially Regulated in Response to Type I IFN

(A) Heatmap of log2-fold changes in IFN-treated cells as compared with mock infected cells. The displayed genes were filtered as described for Figure 2. Genes that are similarly regulated at 6 and 24 h post IFN are clustered together. Data are averages from three biological replicates. Genes missing a gene name and a function in the current Ensembl annotation of *M. lucifugus* were listed by their unique and abbreviated ID numbers:
e.g., "ENSMLUG00000015795" was shortened to "15795."

(B) Venn diagrams showing the numbers of significantly regulated mRNAs at the two time points of IFN treatment.

Literature and database searches were done to find information about these genes that we found to behave like IFNB1. As remarked earlier, the transcriptomes published so far were from either virus-infected or from IFN-treated cells but not from both in parallel. Thus, transcriptomes as well as most studies on individual ISGs could not clearly distinguish between primary (i.e., virus dependent) and secondary (virus-induced IFN) responses to infection, thus impeding a clear distinction of gene expressions that are unique for either of these triggers. Moreover, Ruxolitinib was not used before to systematically study IFN-independent cell responses to virus infection. Hence, we had aimed to clearly differentiate true virus-response genes from conventional ISGs indirectly activated by virus-induced IFN.

The chemokine CCL4 (Macrophage inflammatory protein-β; MIP1-β), an attractant of immune cells such as macrophages or natural killer cells, is not an ISG in humans or other mammals (Shaw et al., 2017). However, CCL4 was found to be upregulated after 24 h of infection with the IFN-inducing NDV in *P. vampyrus* megabat cells (Glennon et al., 2015). Our results show that this occurs independently of IFN signaling.


A
Clone13:IFN
6h 24h
ZBP1 IL4I1 ESIP1 TRIM22 BST2 BST2 IFM2 BST2 TRI34 OAS1 SAMHD1 OAS3 15795 MX2 NT5C3A MX2
IFM2 24605 TRIM5 25786 HRSL4 PSMB9 30476 PARP9 GBP4 24631 26023 PA216 STAT2 PA216 26326 STAT1 1A04 1A04 TAPBPL GBP6 26066 GNB4 27061 NAMPT 13298 CASP1 23420 1A36 1B40 PSMB10
IFNB1 CCL5 CCL4
ABTB2 NEURL3 CHAC1 6397 ADAMTS6 CD40 PPP1R3B TRIB3 NOD2 NUGGC TRIB3 DDIT3 ADM SOX10 SC6A7 SOX9 RFX4 RELB ART4 RGS2 CFAP45 NOXO1 PLK2 GADD45B
KHNYN MFSD12 1A04 507 CASPD 13968 30632 ABI3 1A04 GBP1 UNC93B1 FBXO6 C19orf66 SMAGP 1C01 TPPP DAXX TAP1 PML TRAFD1 PDCD1LG2 PHF11 HERC6 SAMD9L CS012 SP110 GBP6 DDX58 OAS1 GBP6 BTC IFI6 IFI44 RNASEL PA216 GBP4 LGALS3BP SP140 NMI HELZ2 TDRD7 GBP1 P2RY14 6154 GBP1 CYSLTR2 TMTC2
10173 FCAMR NFKB2 RASF5 LAMB3 ICAM1 MMP7 HS3ST1 C3orf70 TAF1D STAC EBI3 ZBTB46 RL12 STRIP2 SLC6A5 12598 NRP2 NFKB1 FOSL1 1508 CDC42EP3 ARRD4 ATF3 TEX14 TAF4B NFKBIA
27952 PARP10 HSH2D GBP1 GBP1 HRSL4 BCL2L15 TRIM5 RN213 SAMD9 24689 UBA7 TCEA3 IFI44L SCNN1G UBP18 DHX58 ISG15 PARP12 BST2 MX1 5691 BCL2L14 11557 IRF7 4321 RSAD2 DDX60 GBP1 NPL OASL FA46A
CDH26 27282 GBP5 CD274 IDO1 ARID5A RSAD2 ETV7 IL15RA SYWC IFIH1 PLEKHA4
NFKBIE ALDH1A3 PTGS2 IKBKE APBA1 PFKFB3 12714 WIPI1 WNT10B 1001 VGF IRAK2
CH25H TNFAIP3 CSF2 CCL2 IFNL3 CXCL11 ICAM4 GROG CXCL10 ADH1 CD83 STEAP4 BIRC3 VCAM1
B
"Down-regulated"
"Up-regulated"
6h
24h
135
0
IFNB1
1
85
C
ENSMLUG00000008021 IFNB1
ENSMLUG00000011369 CCL2
ENSMLUG00000002898 CCL4
ENSMLUG00000013997 IFNL3
ENSMLUG00000015052 CSF2
ENSMLUG00000008622 CH25H
ENSMLUG00000012289 ICAM1
ENSMLUG00000025607 STEAP4
DESeq2 normalized read count
6h 24h 6h 24h 6h 24h
mock Clone 13 IFN
log2 FC
6 4 2 0 −2 −4 −6
treatment
mock
Clone 13
IFN
time point
6h
24h

Figure 4. Genes Differentially Regulated by Virus Infection versus Type I IFN

(A) Heatmap of log2-fold changes in IFN-treated cells as compared with Clone 13-infected cells. The displayed genes were filtered by an absolute log2-fold change of 2 and an adjusted p value < 0.05. Genes that are similarly regulated at 6 and 24 h post IFN are clustered together. Data are averages from three biological replicates. Genes missing a gene name and a function in the current Ensembl annotation of *M. lucifugus* were listed by their unique and abbreviated ID numbers: e.g., "ENSMLUG00000015795" was shortened to "15795."

(B) Venn diagrams showing the numbers of significantly regulated mRNAs at the two time points of IFN treatment.

(C) Expression box plots of selected mRNAs that responded significantly to Clone 13 treatment but not to control and IFN-stimulated conditions. The plots show the DESeq2-normalized expression values for each condition and biological replicate. Graphs show mean values and standard deviations from the three biological replicates.

Thus, we propose CCL4 to be an apparently conserved (humans, megabats, microbats) virus response gene.

The type III interferon IFNL3 (IFNL2/3 in humans) was shown to be stimulated by IRF3 or IRF7 as well as by Sendai virus infection in human (Ank et al., 2006; Osterlund et al., 2007) and by NDV in *P. vampyrus* cells (Glennon et al., 2015). With regard to IFN responsiveness, there are no entries for mice, humans, and other mammals in the databases (Carrasco Pro et al., 2018; Rusinova et al., 2013; Shaw et al., 2017). Our Ruxolitinib data demonstrate that also IFNL3 is a conserved virus-response gene.

CH25H is a powerful broad-spectrum inhibitor of virus entry (Liu et al., 2013; Reboldi et al., 2014). It is not responsive to NDV infection in *P. vampyrus* cells (Glennon et al., 2015). CH25H is published as being weakly IFN stimulated in human (which we could not observe in our A549 cells), rat, horse, and dog; unresponsive to IFN in sheep, pigs and bats; and actually downregulated in cattle (Shaw et al., 2017). Thus, CH25H is a little conserved (and weak) ISG that we find in humans and *M. daubentonii* to be a novel and strong virus-response gene.

STEAP4 is a TNF-α- and IL1β-induced metalloreductase (Kralisch et al., 2009). It is IFN stimulated in humans and pigs but not in any other mammalian species (Shaw et al., 2017). Interestingly, we observed a complete non-responsiveness to any stimulant in human A549 cells, whereas it was upregulated by Clone 13 infection in *M. daubentonii* cells. In *P. vampyrus*, by contrast, it is not among the virus-activated (Glennon et al., 2015).

Thus, taken together, we mapped the global responses of *M. daubentonii* to both virus infection and IFN treatment. Moreover, owing to our statistically robust datasets, early and late time points of sampling, and control experiments using Ruxolitinib, we could identify genes that are like IFNB1 exclusively upregulated by virus infection, either in both humans and *Myotis* (CCL4, IFNL3, CH25H) or only in *Myotis* (STEAP4).

Specific Features of the Microbat Responses

A somewhat surprising finding was the low presence of type I IFN subtypes besides IFNB1. In fact, we could identify only a type I IFN gene with similarity to horse IFNW2 (IFN-ω2) as being modestly IFN stimulated at the 6-h time point, where it reached a log2 fold change of 2.23 and a significant p value (see Figure 3). Another detectable type I IFN subtype (although it did not reach the significance threshold) was a relative to human IFNA5. Also Shaw et al. did not list any type I IFN in their pan-mammal transcriptome study (Shaw et al., 2017), whereas studies in megabats (Pavlovich et al., 2018; Zhou et al., 2016) showed an upregulation of IFN-α- or IFN-ω-like genes upon Sendai virus infection by RT-PCR. Moreover, Zhou et al. reported high base levels of several type I IFN subtypes in the megabat *P. alecto* (Zhou et al., 2016), which was observed neither for the megabat *R. aegyptiacus* (Pavlovich et al., 2018) nor by us in *M. daubentonii* microbat cells.

An interesting feature of our *M. daubentonii* data was the detection of multiple paralogs of Mx and BST2. In the genome of the related *M. lucifugus* we identified three and four copies of Mx and BST2, respectively. Based on the *M. lucifugus* reference genome, *M. daubentonii* significantly upregulated either all three (Mx) or all four (BST2) genes (Figure 6A). Mx (myxovirus resistance protein) is a large cytosolic GTPase with a broad antiviral spectrum (Haller et al., 2015). Almost all investigated vertebrate species express multiple paralogs (Haller et al., 2015). Bat Mx proteins (including Mx1 of *M. daubentonii*) were shown to confer antiviral activity (Fuchs et al., 2017). BST2 (bone marrow stromal cell antigen 2), also called Tetherin, is an antiviral transmembrane protein tethering enveloped virus particles to the plasma membrane (Douglas et al., 2010). A search in the annotated genomes of mammals revealed that *Yangochiroptera/Vespertilionidae* such as *Myotis lucifugus*, *brandtii* und *davidii*, as well as *Eptesicus fuscus* harbor several copies of the

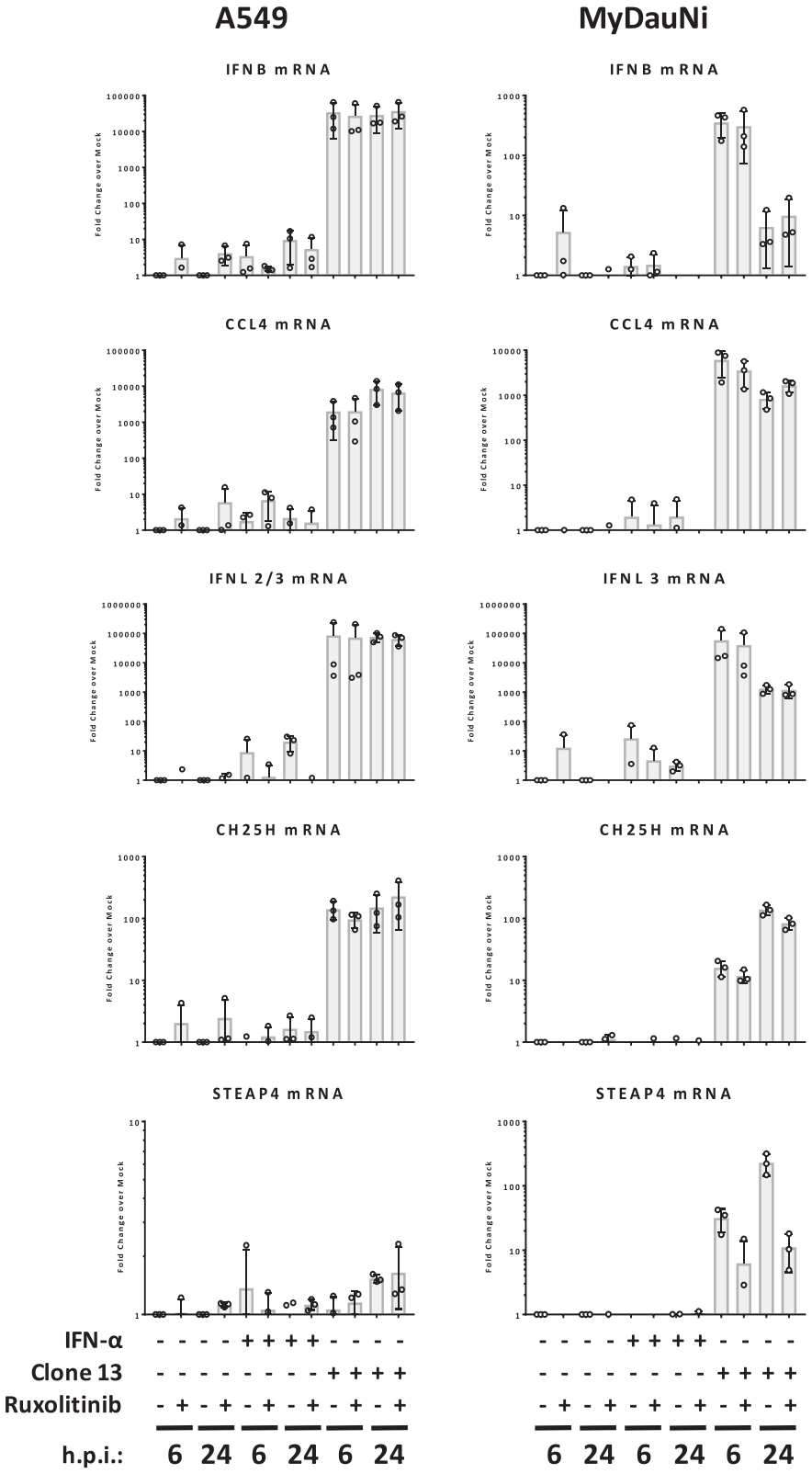
A549
MyDauNi
IFNB mRNA
IFNB mRNA
CCL4 mRNA
CCL4 mRNA
IFNL 2/3 mRNA
IFNL 3 mRNA
CH25H mRNA
CH25H mRNA
STEAP4 mRNA
STEAP4 mRNA
Fold Change over Mock
IFN-α - - - - + + + + - - - -
Clone 13 - - - - - - - - + + + +
Ruxolitinib - + - + - + - + - + - +
h.p.i.: 6 24 6 24 6 24
6 24 6 24 6 24

Figure 5. RT-qPCR Confirmation of Virus-Only Response Genes

Human A549 and *M. daubentonii* MyDauNi cells, treated or not with Ruxolitinib, were incubated with 1,000 U/ml IFN-α or infected with Clone 13 (MOI 5) for 6 or 24 h, respectively. Expression of IFNB1, CCL4, IFNL2/3 (A549)/IFNL3 (MyDauNi), CH25H, and STEAP4 were monitored by RT-qPCR. The graphs show the fold induction over mock, for the respective time point, with mean values and standard deviations from three independent replicates.

BST2 gene, whereas *Miniopterus natalensis* (*Yangochiroptera*/*Miniopteridae*) seems to have just one copy (Figure 6B and data not shown). Using our *M. daubentonii* RNA-seq data, we were able to detect expression of four BST2 paralogs in the genome of *M. lucifugus*. However, two had an identical sequence (data not shown), so we confirm three BST2 paralogs with a differing sequence in the transcriptome of *M. daubentonii*. Thus, *Vespertilionidae* microbats are unique in harboring a multitude of BST2 paralogs, since all other species (except for sheep, which have two [Varela et al., 2017]) have only one copy. Overall, our observations are that *Yangochiroptera*/*Vespertilionidae* microbats express a high number of paralogs of Mx and unexpectedly also BST2, two ISGs with a broad antiviral spectrum. This may indicate an increased capability to directly fend off virus infections.

Comparison with Other Published Innate Immunity Bat Transcriptomes

As mentioned, previous transcriptional profiling studies of bats overwhelmingly used weak IFN inducer viruses or IFN and megabat cells, and only one study so far (again in megabats [Glennon et al., 2015]) used a truly IFN-inducing virus. Moreover, a global, side-by-side comparison between virus- and IFN-stimulated transcriptomes seems not to exist for any species, not even for humans. In addition to the points raised earlier on IFN subtypes and ISGs, we compared some of our findings with the distinctive results from previous bat studies.

Glennon et al. profiled the transcriptome of cells from the megabat *P. vampyrus* infected for 24 h with the IFN-inducing NDV (Glennon et al., 2015). They observed activation of IFNB1 and prototypical ISGs (e.g., DDX58, IFIH1, BST2, Mx1, or ISG15) and identified several novel ISGs, most prominently MORC3 (MORC family CW-type zinc finger 3). Subsequent RT-PCR analyses showed that this novel ISG was not consistently IFN dependent in cells from other bats but was NDV induced in all bat species, including the microbat *Myotis velifer incautus* (Glennon et al., 2015). In the pan-species IFN response comparisons of Shaw et al., MORC3 was identified as a core ISG (Shaw et al., 2017). Also, in our *M. daubentonii* transcriptomes, MORC3 was upregulated by IFN and Clone 13, although only weakly (see https://www.rna.uni-jena.de/supplements/mda/report.html). Interestingly, MORC3 is known as a restriction factor of herpes viruses (Sloan et al., 2016) but a pro-viral factor for influenza virus (Ver et al., 2015).

De la Cruz Vera et al. identified for the megabat *P. alecto* several genes that were not previously reported as being ISGs, namely, EMC2, FILIP1, IL17RC, OTOGL, SLC10A2, SLC24A1, and RNASEL (De La Cruz-Rivera et al., 2018). Our transcriptomes show that EMC2, FILIP1, IL17RC, OTOGL, and SLC24A1/2 are not ISGs in *M. daubentonii*, whereas RNASEL was confirmed. In fact, RNASEL is an ISG in most of the species investigated by Shaw et al. except for humans and chicken (Shaw et al., 2017), thus bolstering the conclusions of de la Cruz Vera et al.. Thus, the microbat ISG profile is distinct from the one of megabats.

Conclusions

Bats, which comprise about 20% of all living mammal species, have recently come into the focus of virus and innate immunity research. However, the group of "bats" is very heterogeneous and encompasses both *Yinpterochiroptera* and *Yangochiroptera*, which have diverged since approximately 60 million years (Teeling et al., 2018). For *Yangochiroptera* microbats, in contrast to megabats of the *Yinpterochiroptera* suborder, the IFN system is only poorly characterized. Here, we presented the time-dependent transcriptional profiles of *M. daubentonii* cells infected with a strong IFN inducer virus or treated with IFN. Our data revealed virus-triggered genes (CCL4, IFNL3, CH25H, STEAP4) that are not regulated by IFN itself, as well as the presence of multiple paralogs of directly antiviral ISGs such as Mx and BST2. CCL4 and IFNL3 attract immune cells and enhance local antiviral activity, respectively, and Mx, BST2, and CH25H are broad-spectrum virus inhibitors. Although our data are derived from a single cell line and may not be entirely generalizable, our analysis indicates that the *Yangochiroptera* microbat IFN system may exhibit features not observed for megabats or humans (STEAP4 as virus-response gene, at least 3 BST2 paralogs). Moreover, we report the absence of a series of megabat ISGs (EMC2, FILIP1,

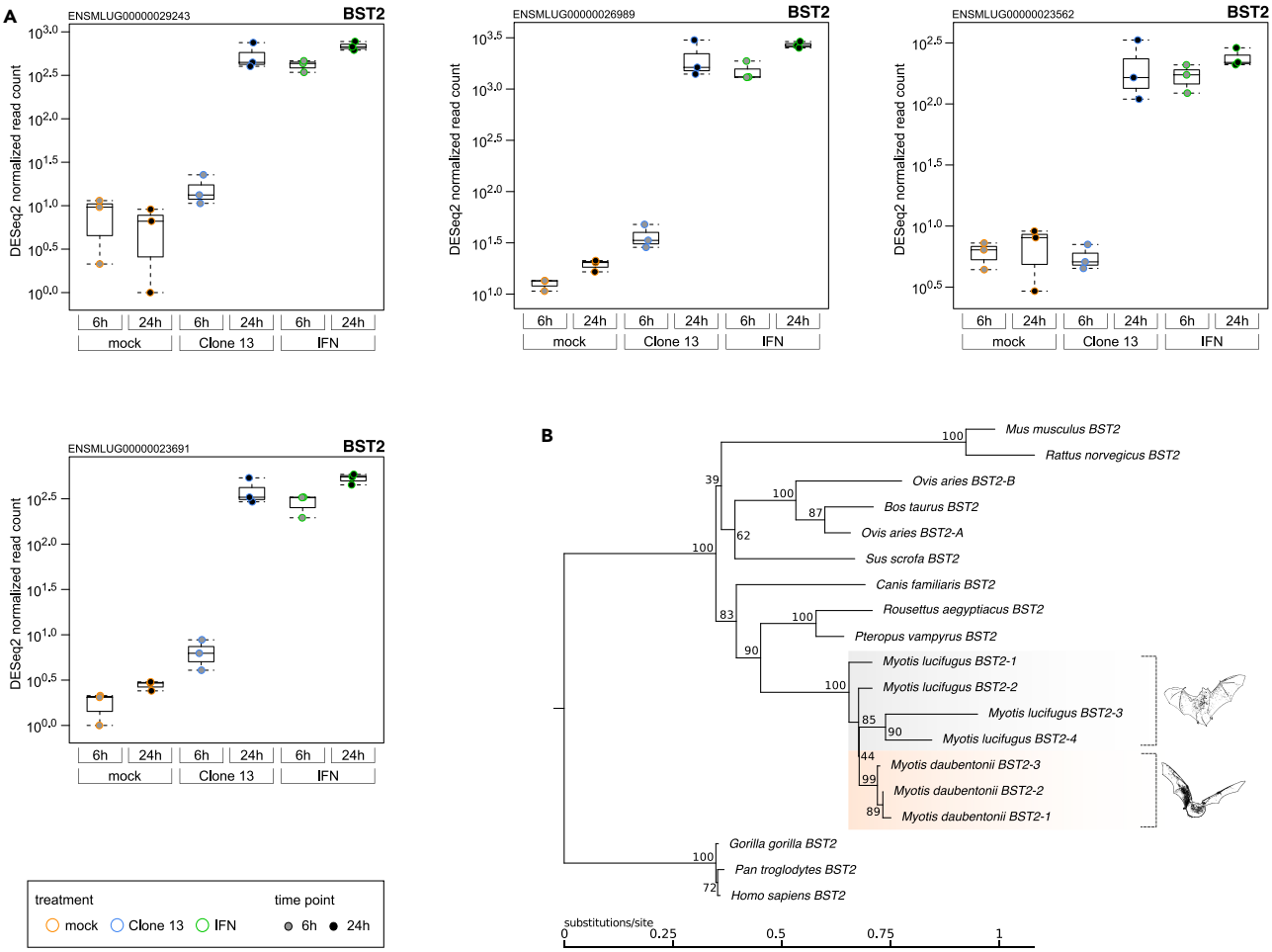

Figure 6. BST2 Paralogs and Phylogeny

We identified four BST2 paralogous genes in the genome of *M. lucifugus* that served as a reference in this study. From the *de novo* transcriptome assembly of the *M. daubentonii* RNA-seq data, we were able to distinguish only three different BST2-like mRNAs.

(A) The box plots show arithmetic means and standard deviations from the DESeq2-normalized expression values of the *M. daubentonii* RNA-seq reads, uniquely mapped to the *M. lucifugus* reference genome.

(B) Phylogenetic tree of twelve selected mammalian BST2 genes and the four and three BST2 paralogs identified in the *M. lucifugus* genome or *M. daubentonii* transcriptome, respectively.

IL17RC, OTOGL, SLC24A1) and confirm a set of ISGs as being conserved also in *Yangochiroptera*. Also, in contrast to findings in megabat cells, we could not detect an increased copy number or upregulation of type I IFN genes other than IFNB1, or unusually high base levels of IFNs. Moreover, based on true biological replicates we offer statistically robust RNA-seq data on a time-resolved comparison between virus-induced and IFN-stimulated transcriptional responses of an IFN competent mammalian cell line.

Limitations of the Study

Potential caveats of our paper are that (1) an immortalized *Myotis daubentonii* cell line was used, (2) the *Myotis daubentonii* cells are of kidney origin and their IFN response were compared with that of a human lung cell line, and (3) it is unknown how much the innate immune response of *Myotis* cells are representative for the entire suborder *Yangochiroptera*.

METHODS

All methods can be found in the accompanying Transparent Methods supplemental file.

DATA AND CODE AVAILABILITY

Our online search tool is available at https://www.rna.uni-jena.de/supplements/mda/report.html. The raw read data was deposited in the GEO database under accession number GEO: GSE121301. All intermediate files such as the quality-trimmed and rRNA-cleaned reads of all 18 samples, mappings, the extended genome annotation, and raw read counts were uploaded to the Open Science Framework under https://doi.org/10.17605/OSF.IO/X9KAD.

Supplemental figures and files are also found at https://www.rna.uni-jena.de/supplements/mda/.

https://www.rna.uni-jena.de/supplements/mda/.

SUPPLEMENTAL INFORMATION

Supplemental Information can be found online at https://doi.org/10.1016/j.isci.2019.08.016.

ACKNOWLEDGMENTS

We thank Ivonne Görlich and Marco Groth from the Core Facility DNA sequencing of the Leibniz Institute on Aging, Fritz Lipmann Institute in Jena for their help with RNA sequencing, Bernd Schmeck for analyzing RNA integrity, and Georg Kochs and Alejandro Brun for kindly providing antibodies. Work in the F.W. laboratory is funded by the Deutsche Forschungsgemeinschaft (DFG, German Research Foundation) – Projektnummer 197785619 – SFB 1021 and by SPP 1596 (grant numbers We 2616/7-1, We 2616/7-2), by the RAPID consortium of the Bundesministerium für Bildung und Forschung (BMBF, grant number 01KI1723E), and by the LOEWE-Schwerpunkt "Medical RNomics" of the Land Hessen. M.M. and M.H. are supported by the DFG SPP 1596. Work in the laboratory of C.D. was supported by the DFG grant SPP 1596 (grant number DR 772/10-2) and by the RAPID consortium of the BMBF (grant number 01KI1723A). Funding for open access charge: DFG SPP 1596 (grant number We 2616/7-2).

AUTHOR CONTRIBUTIONS

Conceptualization, M.H., A.S., M.A.M., C.D., M.M., and F.W.; Methodology, M.H., A.S., J.W., M.A.M., C.D., M.M., and F.W.; Software, M.H. and M.M.; Validation, A.S. and F.W.; Formal Analysis, M.H. and F.W.; Investigation, M.H., A.S., J.W., and M.A.M.; Resources, C.D., M.M., and F.W.; Data Curation, M.H. and M.M.; Writing – Original Draft, F.W.; Writing – Review & Editing, M.H., A.S., M.A.M., M.M., and F.W.; Supervision, M.M. and F.W.; Project Administration, F.W.; Funding Acquisition, C.D., M.M., and F.W.

DECLARATION OF INTERESTS

The authors declare no competing interests.

Received: February 14, 2019
Revised: July 10, 2019
Accepted: August 7, 2019
Published: September 27, 2019

REFERENCES

Ank, N., West, H., Bartholdy, C., Eriksson, K., Thomsen, A.R., and Paludan, S.R. (2006). Lambda interferon (IFN-lambda), a type III IFN, is induced by viruses and IFNs and displays potent antiviral activity against select virus infections in vivo. J. Virol. *80*, 4501–4509.

Balogh, A., Bator, J., Marko, L., Nemeth, M., Pap, M., Setalo, G., Jr., Muller, D.N., Csatary, L.K., and Szeberenyi, J. (2014). Gene expression profiling in PC12 cells infected with an oncolytic Newcastle disease virus strain. Virus Res. *185*, 10–22.

Bankevich, A., Nurk, S., Antipov, D., Gurevich, A.A., Dvorkin, M., Kulikov, A.S., Lesin, V.M., Nikolenko, S.I., Pham, S., Prjibelski, A.D., et al. (2012). SPAdes: a new genome assembly algorithm and its applications to single-cell sequencing. J. Comput. Biol. *19*, 455–477.

Billecocq, A., Spiegel, M., Vialat, P., Kohl, A., Weber, F., Bouloy, M., and Haller, O. (2004). NSs protein of Rift Valley fever virus blocks interferon production by inhibiting host gene transcription. J. Virol. *78*, 9798–9806.

Calisher, C.H., Childs, J.E., Field, H.E., Holmes, K.V., and Schountz, T. (2006). Bats: important reservoir hosts of emerging viruses. Clin. Microbiol. Rev. *19*, 531–545.

Carrasco Pro, S., Dafonte Imedio, A., Santoso, C.S., Gan, K.A., Sewell, J.A., Martinez, M., Sereda, R., Mehta, S., and Fuxman Bass, J.I. (2018). Global landscape of mouse and human cytokine transcriptional regulation. Nucleic Acids Res. *46*, 9321–9337.

De La Cruz-Rivera, P.C., Kanchwala, M., Liang, H., Kumar, A., Wang, L.F., Xing, C., and Schoggins, J.W. (2018). The IFN response in bats displays distinctive IFN-stimulated gene expression kinetics with atypical RNASEL induction. J. Immunol. *200*, 209–217.

Dobin, A., and Gingeras, T.R. (2015). Mapping RNA-seq reads with STAR. Curr. Protoc. Bioinformatics *51*, 11.14.1–19.

Dobson, A.P. (2005). What links bats to emerging infectious diseases? Science *310*, 628–629.

Doganay, S., Lee, M.Y., Baum, A., Peh, J., Hwang, S.Y., Yoo, J.Y., Hergenrother, P.J., Garcia-Sastre, A., Myong, S., and Ha, T. (2017). Single-cell analysis of early antiviral gene expression reveals a determinant of stochastic IFNB1 expression. Integr. Biol. (Camb). *9*, 857–867.

Douglas, J.L., Gustin, J.K., Viswanathan, K., Mansouri, M., Moses, A.V., and Fruh, K. (2010). The great escape: viral strategies to counter BST-2/tetherin. PLoS Pathog. *6*, e1000913.

Drexler, J.F., Corman, V.M., Muller, M.A., Maganga, G.D., Vallo, P., Binger, T., Gloza-Rausch, F., Cottontail, V.M., Rasche, A., Yordanov, S., et al. (2012). Bats host major mammalian paramyxoviruses. Nat. Commun. *3*, 796.

Drexler, J.F., Corman, V.M., Wegner, T., Tateno, A.F., Zerbinati, R.M., Gloza-Rausch, F., Seebens, A., Muller, M.A., and Drosten, C. (2011). Amplification of emerging viruses in a bat colony. Emerg. Infect. Dis. *17*, 449–456.

Fu, L., Niu, B., Zhu, Z., Wu, S., and Li, W. (2012). CD-HIT: accelerated for clustering the next-generation sequencing data. Bioinformatics *28*, 3150–3152.

Fuchs, J., Hölzer, M., Schilling, M., Patzina, C., Schoen, A., Hoenen, T., Zimmer, G., Marz, M., Weber, F., Muller, M.A., et al. (2017). Evolution and antiviral specificities of interferon-induced Mx proteins of bats against ebola, influenza, and other RNA viruses. J. Virol. *91*, e00361–17.

Garcin, G., Bordat, Y., Chuchana, P., Monneron, D., Law, H.K., Piehler, J., and Uze, G. (2013). Differential activity of type I interferon subtypes for dendritic cell differentiation. PLoS One *8*, e58465.

Gerrard, D.L., Hawkinson, A., Sherman, T., Modahl, C.M., Hume, G., Campbell, C.L., Schountz, T., and Frietze, S. (2017). Transcriptomic signatures of tacaribe virus-infected jamaican fruit bats. mSphere *2*, 245–17.

Glennon, N.B., Jabado, O., Lo, M.K., and Shaw, M.L. (2015). Transcriptome profiling of the virus-induced innate immune response in pteropus vampyrus and its attenuation by nipah virus interferon antagonist functions. J. Virol. *89*, 7550–7566.

Grabherr, M.G., Haas, B.J., Yassour, M., Levin, J.Z., Thompson, D.A., Amit, I., Adiconis, X., Fan, L., Raychowdhury, R., Zeng, Q.D., et al. (2011). Full-length transcriptome assembly from RNA-Seq data without a reference genome. Nat. Biotechnol. *29*, 644–U130.

Grandvaux, N., Servant, M.J., tenOever, B., Sen, G.C., Balachandran, S., Barber, G.N., Lin, R.T., and Hiscott, J. (2002). Transcriptional profiling of interferon regulatory factor 3 target genes: direct involvement in the regulation of interferon-stimulated genes. J. Virol. *76*, 5532–5539.

Haller, O., Staeheli, P., Schwemmle, M., and Kochs, G. (2015). Mx GTPases: dynamin-like antiviral machines of innate immunity. Trends Microbiol. *23*, 154–163.

Hamming, O.J., Gad, H.H., Paludan, S., and Hartmann, R. (2010). Lambda interferons: new cytokines with old functions. Pharmaceuticals (Basel) *3*, 795–809.

Hess, R.D., Weber, F., Watson, K., and Schmitt, S. (2012). Regulatory, biosafety and safety challenges for novel cells as substrates for human vaccines. Vaccine *30*, 2715–2727.

Hölzer, M., Krahling, V., Amman, F., Barth, E., Bernhart, S.H., Carmelo, V.A., Collatz, M., Doose, G., Eggenhofer, F., Ewald, J., et al. (2016). Differential transcriptional responses to Ebola and Marburg virus infection in bat and human cells. Sci. Rep. *6*, 34589.

Hölzer, M., and Marz, M. (2019). De novo transcriptome assembly: A comprehensive cross-species comparison of short-read RNA-Seq assemblers. Gigascience *8* (5), giz039.

Huntley, M.A., Larson, J.L., Chaivorapol, C., Becker, G., Lawrence, M., Hackney, J.A., and Kaminker, J.S. (2013). ReportingTools: an automated result processing and presentation toolkit for high-throughput genomic analyses. Bioinformatics *29*, 3220–3221.

Jilg, N., Lin, W., Hong, J., Schaefer, E.A., Wolski, D., Meixong, J., Goto, K., Brisac, C., Chusri, P., Fusco, D.N., et al. (2014). Kinetic differences in the induction of interferon stimulated genes by interferon-alpha and interleukin 28B are altered by infection with hepatitis C virus. Hepatology *59*, 1250–1261.

Jordan, I., Horn, D., Oehmke, S., Leendertz, F.H., and Sandig, V. (2009). Cell lines from the Egyptian fruit bat are permissive for modified vaccinia Ankara. Virus Res. *145*, 54–62.

Kopylova, E., Noe, L., and Touzet, H. (2012). SortMeRNA: fast and accurate filtering of ribosomal RNAs in metatranscriptomic data. Bioinformatics *28*, 3211–3217.

Kralisch, S., Sommer, G., Weise, S., Lipfert, J., Lossner, U., Kamprad, M., Schrock, K., Bluher, M., Stumvoll, M., and Fasshauer, M. (2009). Interleukin-1beta is a positive regulator of TIARP/STAMP2 gene and protein expression in adipocytes in vitro. FEBS Lett. *583*, 1196–1200.

Kuri, T., Habjan, M., Penski, N., and Weber, F. (2010). Species-independent bioassay for sensitive quantification of antiviral type I interferons. Virol. J. *7*, 50.

Kuzmin, I.V., Schwarz, T.M., Ilinykh, P.A., Jordan, I., Ksiazek, T.G., Sachidanandam, R., Basler, C.F., and Bukreyev, A. (2017). Innate immune responses of bat and human cells to filoviruses: commonalities and distinctions. J. Virol. *91*, e02471–16.

Liu, J., Li, G., Chang, Z., Yu, T., Liu, B., McMullen, R., Chen, P., and Huang, X. (2016). BinPacker: packing-based de novo transcriptome assembly from RNA-seq data. PLoS Comput. Biol. *12*, e1004772.

Liu, S.Y., Aliyari, R., Chikere, K., Li, G., Marsden, M.D., Smith, J.K., Pernet, O., Guo, H., Nusbaum, R., Zack, J.A., et al. (2013). Interferon-inducible cholesterol-25-hydroxylase broadly inhibits viral entry by production of 25-hydroxycholesterol. Immunity *38*, 92–105.

Love, M.I., Huber, W., and Anders, S. (2014). Moderated estimation of fold change and dispersion for RNA-seq data with DESeq2. Genome Biol. *15*, 550.

McElhinney, L.M., Marston, D.A., Wise, E.L., Freuling, C.M., Bourhy, H., Zanoni, R., Moldal, T., Kooi, E.A., Neubauer-Juric, A., Nokireki, T., et al. (2018). Molecular epidemiology and evolution of european bat lyssavirus 2. Int. J. Mol. Sci. *19*, E156.

McWhirter, S.M., Fitzgerald, K.A., Rosains, J., Rowe, D.C., Golenbock, D.T., and Maniatis, T. (2004). IFN-regulatory factor 3-dependent gene expression is defective in Tbk1-deficient mouse embryonic fibroblasts. Proc. Natl. Acad. Sci. U S A *101*, 233–238.

Mostafavi, S., Yoshida, H., Moodley, D., LeBoite, H., Rothamel, K., Raj, T., Ye, C.J., Chevrier, N., Zhang, S.Y., Feng, T., et al. (2016). Parsing the interferon transcriptional network and its disease associations. Cell *164*, 564–578.

Muller, M.A., Devignot, S., Lattwein, E., Corman, V.M., Maganga, G.D., Gloza-Rausch, F., Binger, T., Vallo, P., Emmerich, P., Cottontail, V.M., et al. (2016). Evidence for widespread infection of African bats with Crimean-Congo hemorrhagic fever-like viruses. Sci. Rep. *6*, 26637.

Muller, M.A., Raj, V.S., Muth, D., Meyer, B., Kallies, S., Smits, S.L., Wollny, R., Bestebroer, T.M., Specht, S., Suliman, T., et al. (2012). Human coronavirus EMC does not require the SARS-coronavirus receptor and maintains broad replicative capability in mammalian cell lines. MBio *3*, e00515–12.

Oelofsen, M.J., and Van der Ryst, E. (1999). Could bats act as a reservoir hosts for Rift Valley fever virus? Onderstepoort J. Vet. Res. *66*, 51–54.

Ondov, B.D., Bergman, N.H., and Phillippy, A.M. (2011). Interactive metagenomic visualization in a Web browser. BMC Bioinformatics *12*, 385.

Osterlund, P.I., Pietilae, T.E., Veckman, V., Kotenko, S.V., and Julkunen, I. (2007). IFN regulatory factor family members differentially regulate the expression of type III IFN (IFN-lambda) genes. J. Immunol. *179*, 3434–3442.

Ounit, R., Wanamaker, S., Close, T.J., and Lonardi, S. (2015). CLARK: fast and accurate classification of metagenomic and genomic sequences using discriminative k-mers. BMC Genomics *16*, 236.

Pavlovich, S.S., Lovett, S.P., Koroleva, G., Guito, J.C., Arnold, C.E., Nagle, E.R., Kulcsar, K., Lee, A., Thibaud-Nissen, F., Hume, A.J., et al. (2018). The Egyptian rousette genome reveals unexpected features of bat antiviral immunity. Cell *173*, 1098–1110.e18.

Puthia, M., Ambite, I., Cafaro, C., Butler, D., Huang, Y., Lutay, N., Rydstrom, G., Gullstrand, B., Swaminathan, B., Nadeem, A., et al. (2016). IRF7 inhibition prevents destructive innate immunity-A target for nonantibiotic therapy of bacterial infections. Sci. Transl. Med. *8*, 336ra359.

Reboldi, A., Dang, E.V., McDonald, J.G., Liang, G., Russell, D.W., and Cyster, J.G. (2014). Inflammation. 25-Hydroxycholesterol suppresses interleukin-1-driven inflammation downstream of type I interferon. Science *345*, 679–684.

Rusinova, I., Forster, S., Yu, S., Kannan, A., Masse, M., Cumming, H., Chapman, R., and Hertzog, P.J.

(2013). Interferome v2.0: an updated database of annotated interferon-regulated genes. Nucleic Acids Res. *41*, D1040–D1046.

Schmid, S., Mordstein, M., Kochs, G., Garcia-Sastre, A., and Tenoever, B.R. (2010). Transcription factor redundancy ensures induction of the antiviral state. J. Biol. Chem. *285*, 42013–42022.

Schmieder, R., and Edwards, R. (2011). Quality control and preprocessing of metagenomic datasets. Bioinformatics *27*, 863–864.

Schoggins, J.W. (2014). Interferon-stimulated genes: roles in viral pathogenesis. Curr. Opin. Virol. *6*, 40–46.

Shaw, A.E., Hughes, J., Gu, Q., Behdenna, A., Singer, J.B., Dennis, T., Orton, R.J., Varela, M., Gifford, R.J., Wilson, S.J., et al. (2017). Fundamental properties of the mammalian innate immune system revealed by multispecies comparison of type I interferon responses. PLoS. Biol. *15*, e2004086.

Sloan, E., Orr, A., and Everett, R.D. (2016). MORC3, a component of PML nuclear bodies, has a role in restricting herpes simplex virus 1 and human cytomegalovirus. J. Virol. *90*, 8621–8633.

Stewart, C.E., Randall, R.E., and Adamson, C.S. (2014). Inhibitors of the interferon response enhance virus replication in vitro. PLoS One *9*, e112014.

Teeling, E.C., Vernes, S.C., Davalos, L.M., Ray, D.A., Gilbert, M.T.P., Myers, E., and Bat, K.C. (2018). Bat biology, genomes, and the Bat1K project: to generate chromosome-level genomes for all living bat species. Annu. Rev. Anim. Biosci. *6*, 23–46.

Varela, M., Piras, I.M., Mullan, C., Shi, X., Tilston-Lunel, N.L., Pinto, R.M., Taggart, A., Welch, S.R., Neil, S.J.D., Kreher, F., et al. (2017). Sensitivity to BST-2 restriction correlates with Orthobunyavirus host range. Virology *509*, 121–130.

Varemo, L., Nielsen, J., and Nookaew, I. (2013). Enriching the gene set analysis of genome-wide data by incorporating directionality of gene expression and combining statistical hypotheses and methods. Nucleic Acids Res. *41*, 4378–4391.

Ver, L.S., Marcos-Villar, L., Landeras-Bueno, S., Nieto, A., and Ortin, J. (2015). The cellular factor NXP2/MORC3 is a positive regulator of influenza virus multiplication. J. Virol. *89*, 10023–10030.

Weber, M., Sediri, H., Felgenhauer, U., Binzen, I., Banfer, S., Jacob, R., Brunotte, L., Garcia-Sastre, A., Schmid-Burgk, J.L., Schmidt, T., et al. (2015). Influenza virus adaptation PB2-627K modulates nucleocapsid inhibition by the pathogen sensor RIG-I. Cell Host Microbe *17*, 309–319.

Weiss, S., Witkowski, P.T., Auste, B., Nowak, K., Weber, N., Fahr, J., Mombouli, J.V., Wolfe, N.D., Drexler, J.F., Drosten, C., et al. (2012). Hantavirus in bat, Sierra Leone. Emerg. Infect. Dis. *18*, 159–161.

Wu, L., Zhou, P., Ge, X., Wang, L.F., Baker, M.L., and Shi, Z. (2013). Deep RNA sequencing reveals complex transcriptional landscape of a bat adenovirus. J. Virol. *87*, 503–511.

Wynne, J.W., Shiell, B.J., Marsh, G.A., Boyd, V., Harper, J.A., Heesom, K., Monaghan, P., Zhou, P., Payne, J., Klein, R., et al. (2014). Proteomics informed by transcriptomics reveals Hendra virus sensitizes bat cells to TRAIL-mediated apoptosis. Genome Biol. *15*, 532.

Wynne, J.W., and Wang, L.F. (2013). Bats and viruses: friend or foe? PLoS Pathog. *9*, e1003651.

Xie, Y., Wu, G., Tang, J., Luo, R., Patterson, J., Liu, S., Huang, W., He, G., Gu, S., Li, S., et al. (2014). SOAPdenovo-Trans: de novo transcriptome assembly with short RNA-Seq reads. Bioinformatics *30*, 1660–1666.

Yan, W.D. (2015). Going batty: studying natural reservoirs to inform drug development. Nat. Med. *21*, 831–833.

Yang, S., Zhan, Y., Zhou, Y.J., Jiang, Y.F., Zheng, X.C., Yu, L.X., Tong, W., Gao, F., Li, L.W., Huang, Q.F., et al. (2016). Interferon regulatory factor 3 is a key regulation factor for inducing the expression of SAMHD1 in antiviral innate immunity. Sci. Rep. *6*, 29665.

Zhang, G.J., Cowled, C., Shi, Z.L., Huang, Z.Y., Bishop-Lilly, K.A., Fang, X.D., Wynne, J.W., Xiong, Z.Q., Baker, M.L., Zhao, W., et al. (2013). Comparative analysis of bat genomes provides insight into the evolution of flight and immunity. Science *339*, 456–460.

Zhang, Q., Zeng, L.P., Zhou, P., Irving, A.T., Li, S., Shi, Z.L., and Wang, L.F. (2017). IFNAR2-dependent gene expression profile induced by IFN-alpha in *Pteropus alecto* bat cells and impact of IFNAR2 knockout on virus infection. PLoS One *12*, e0182866.

Zhou, P., Tachedjian, M., Wynne, J.W., Boyd, V., Cui, J., Smith, I., Cowled, C., Ng, J.H., Mok, L., Michalski, W.P., et al. (2016). Contraction of the type I IFN locus and unusual constitutive expression of IFN-alpha in bats. Proc. Natl. Acad. Sci. U S A *113*, 2696–2701.

ISCI, Volume *19*

Supplemental Information

Virus- and Interferon Alpha-Induced Transcriptomes of Cells from the Microbat *Myotis daubentonii*

Martin Hölzer, Andreas Schoen, Julia Wulle, Marcel A. Müller, Christian Drosten, Manja Marz, and Friedemann Weber

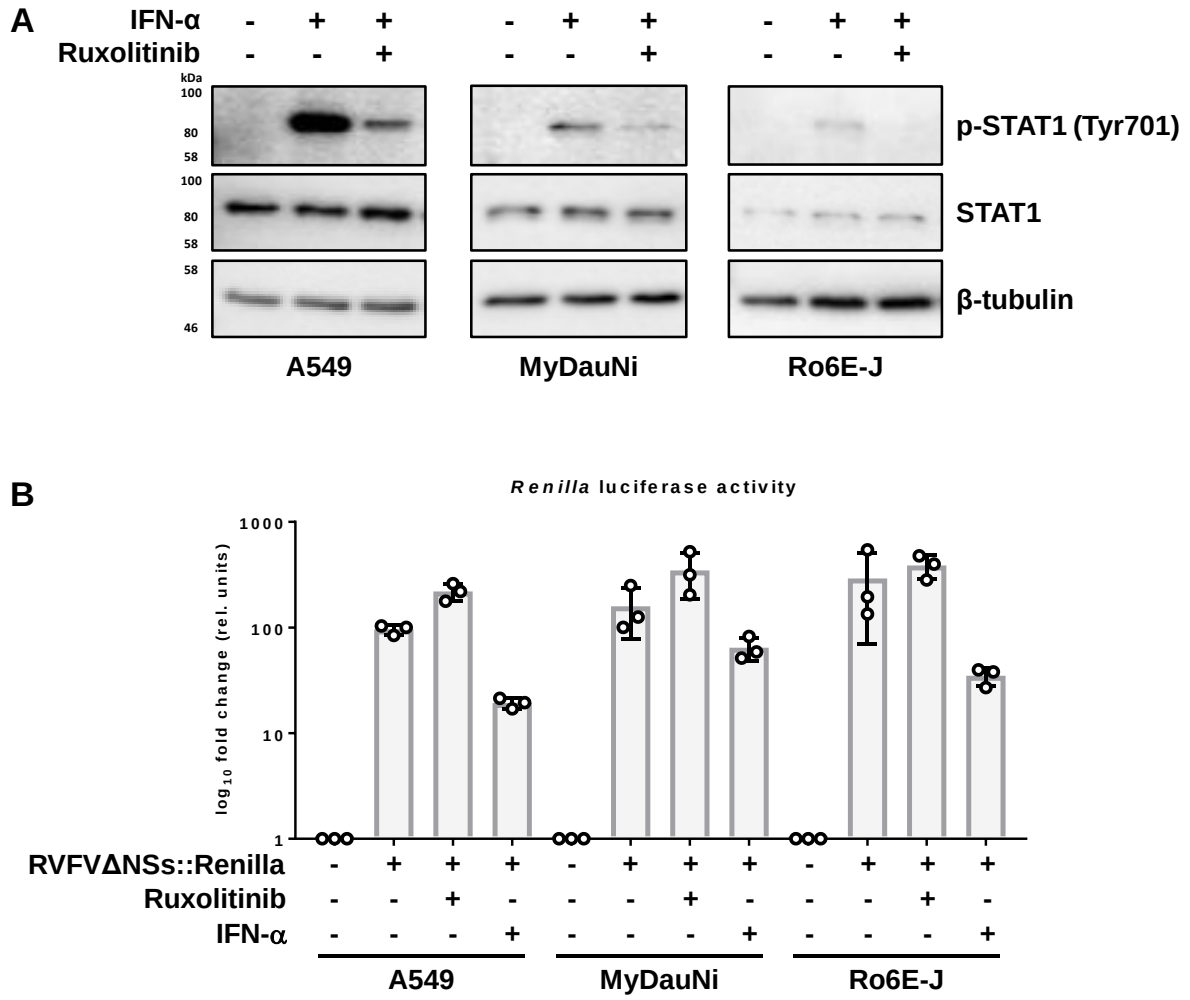

Figure S1, related to Figure 1. *Myotis daubentonii* kidney cell line MyDauNi/2c is fully IFN competent. (A) STAT1-dependent response to exogenous IFN. Human A549, *M. daubentonii* MyDauNi and *R. aegytiacus* Ro6E-J cells where treated with IFN-α, the JAK1/2 inhibitor Ruxolitinib, or were left untreated. Immunoblot analysis was performed with antibodies against the indicated antigens. Representative data from three independent experiments are shown. (B) Multiplication of an IFN-sensitive virus. Cells were pretreated with IFN or Ruxolitinib, infected with the IFN inducing and IFN-sensitive RVFVΔNSs::Renilla, and virus replication was measured by Renilla luciferase assays after 48 h of incubation. The graph shows the virus reporter activities normalized to uninfected background values for each cell line. Mean values and standard deviations from three independent replicates are shown.

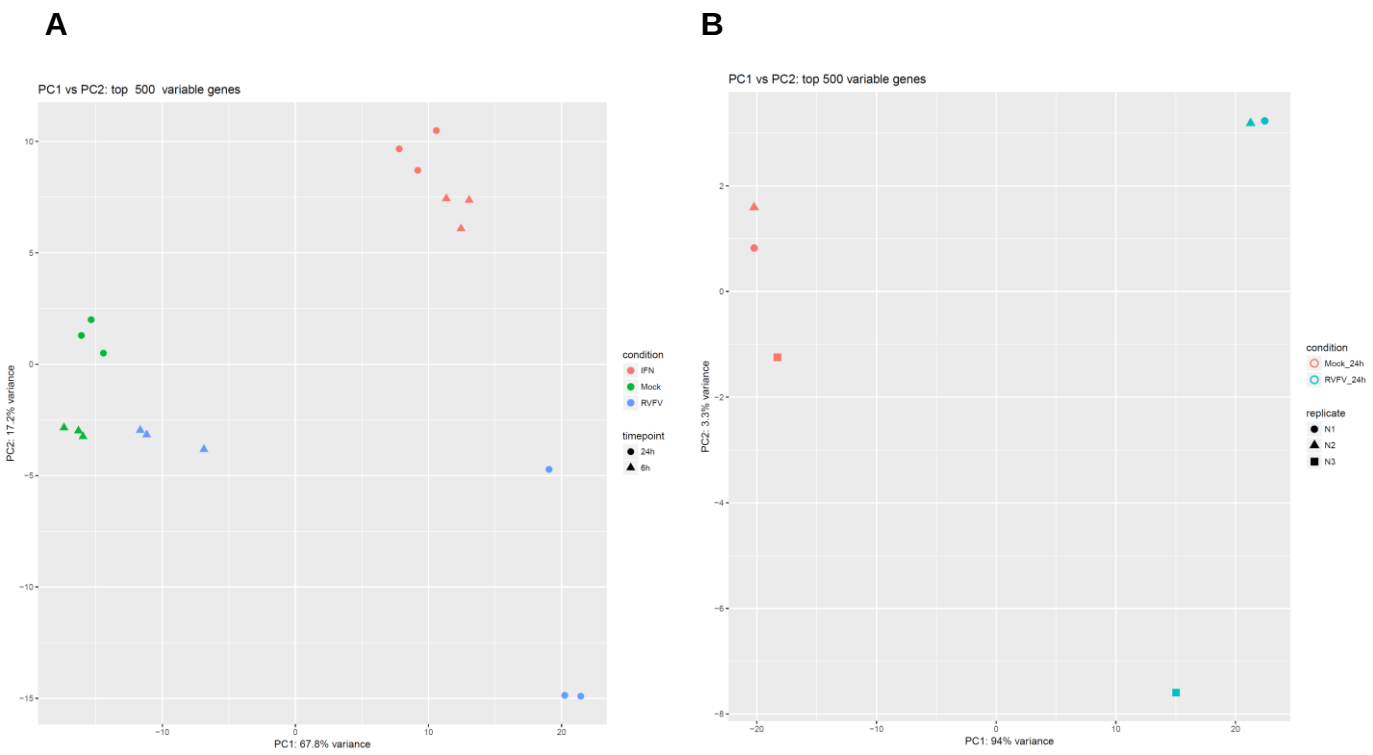

Figure S2, related to Figure 1. Principal component analysis. (A) PCA transformation based on the top 500 variant genes over all samples. One of the 24h RVFV mutant (Clone 13) samples seems to not cluster that well with the other replicates. (B) PCA transformation based on the top 500 variant genes between mock 24h and RVFV mutant 24h samples. The difference between the "outlier" virus-infected sample and the other two replicates accounts only for 3.3% (PC2) of the whole variation in the gene expression data.

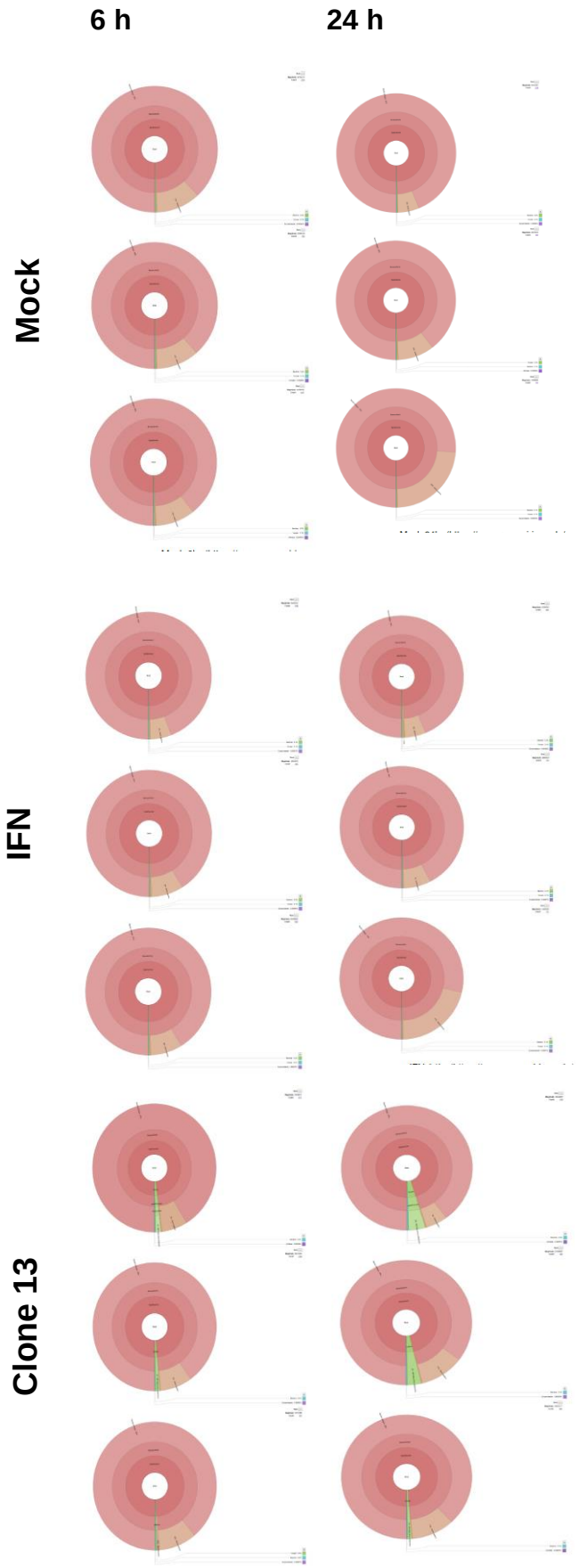

Figure S3, related to Figure 1. CLARK classification was run against NCBI RefSeq genomes of bacteria, viruses, fungi, human and a custom database comprising the *M. lucifugus* genome.

A

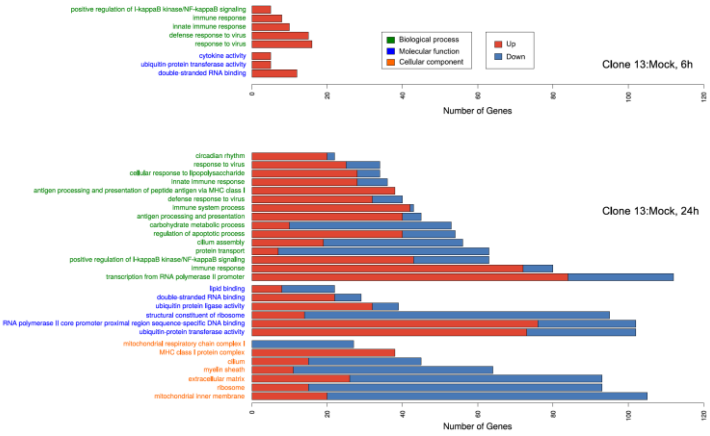

B

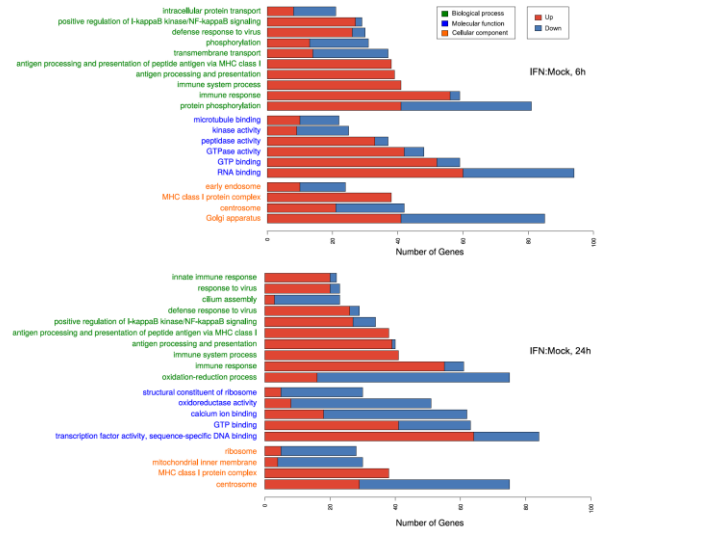

C

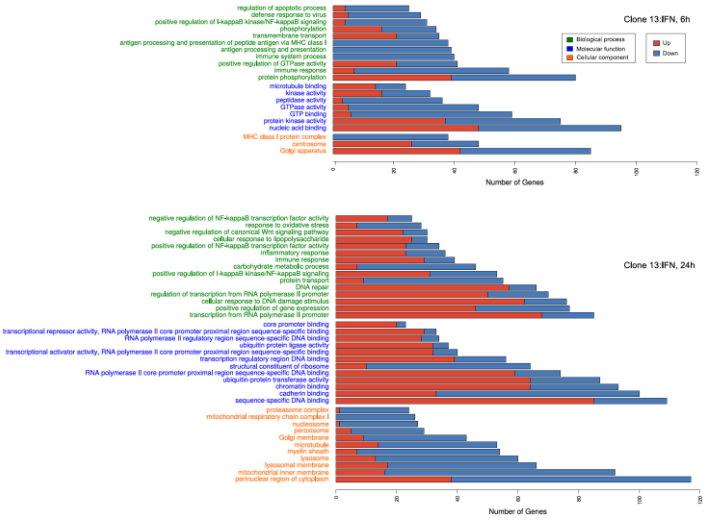

Figure S4, related to Figures 1, 2, 3, 4. Enriched GO terms based on pairwise comparisons. A: Mock vs. Clone13, B: Mock vs. IFN, C: IFN vs. Clone13.

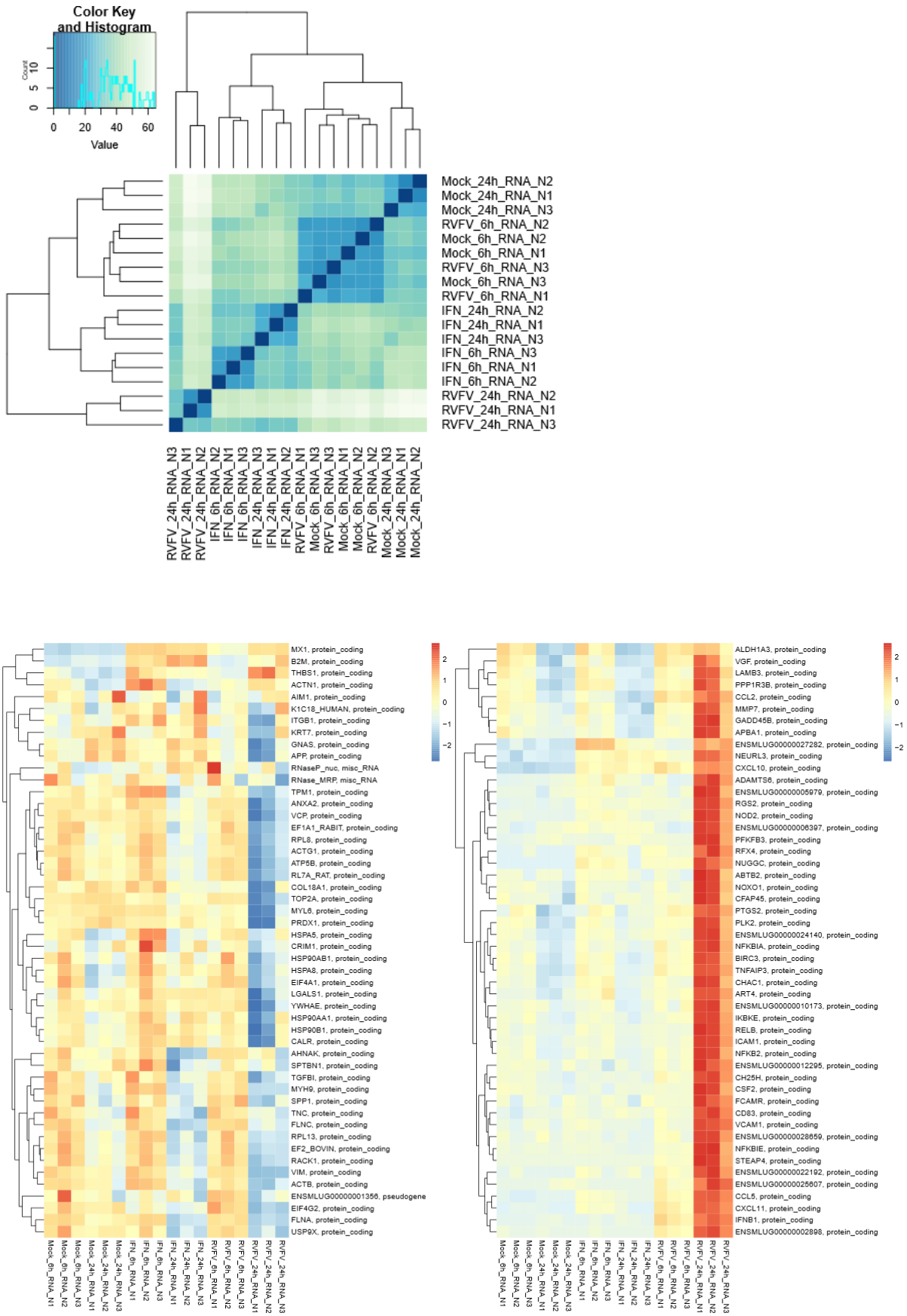

Figure S5, related to Figures 2, 3, and 4. DEG overview.

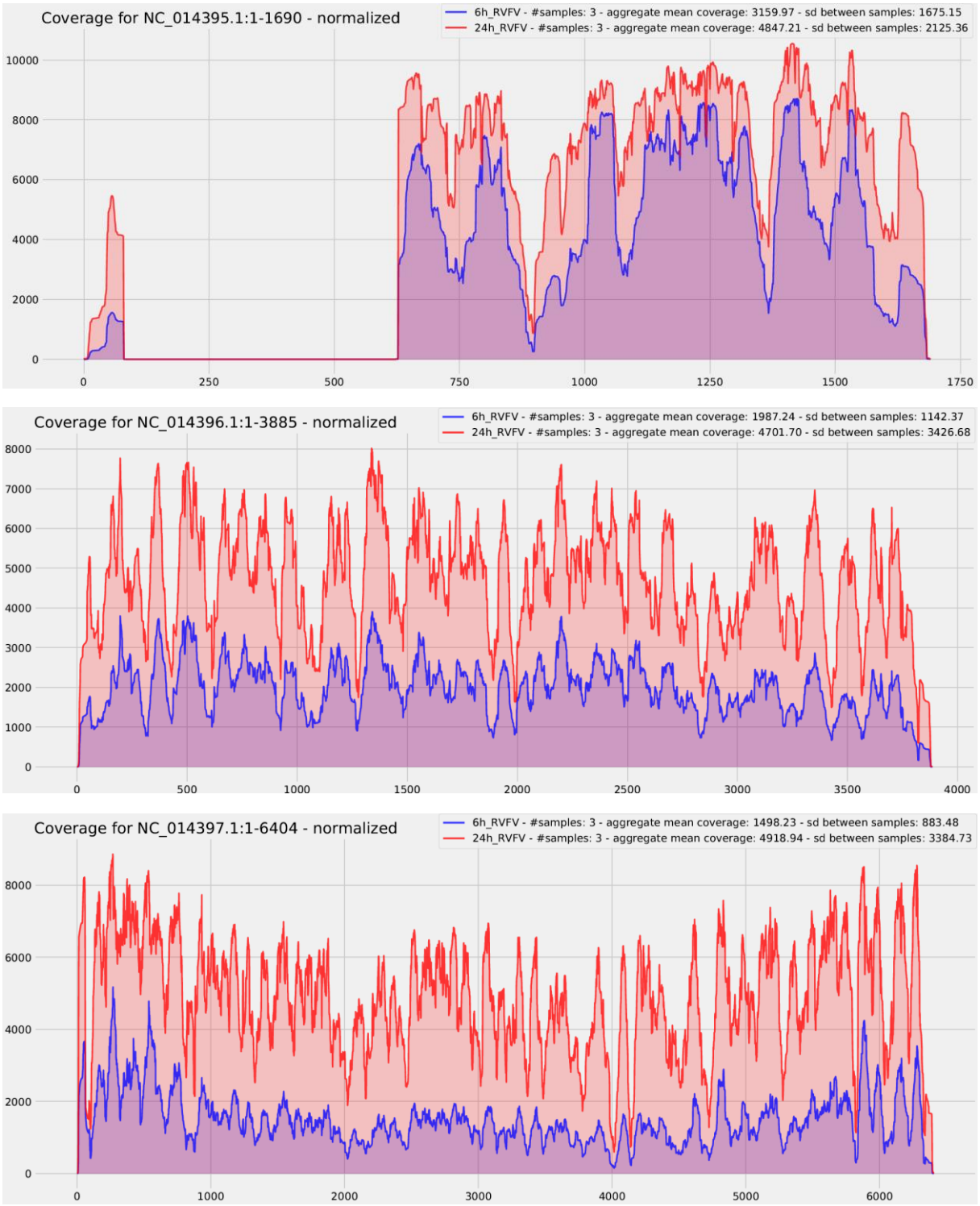

Figure S6, related to Figures 1, 2, 4. Coverage of the S, M, and L segment of the RVFV reference genome. Reference sequences for Clone 13 of the S, M, and L segment of RVFV were downloaded from the NCBI under RefSeq accessions Genbank: NC_014395.1 (S segment), Genbank: NC_014396.1 (M segment), Genbank: NC_014397.1 (L segment). The plots show the aggregate average coverage for the triplicates 6h and 24h post infection with the RVFV Clone13 mutant. Please note the Clone 13-specific deletion in the IFN antagonist NSs on the S segment that determines its high IFN induction capability.

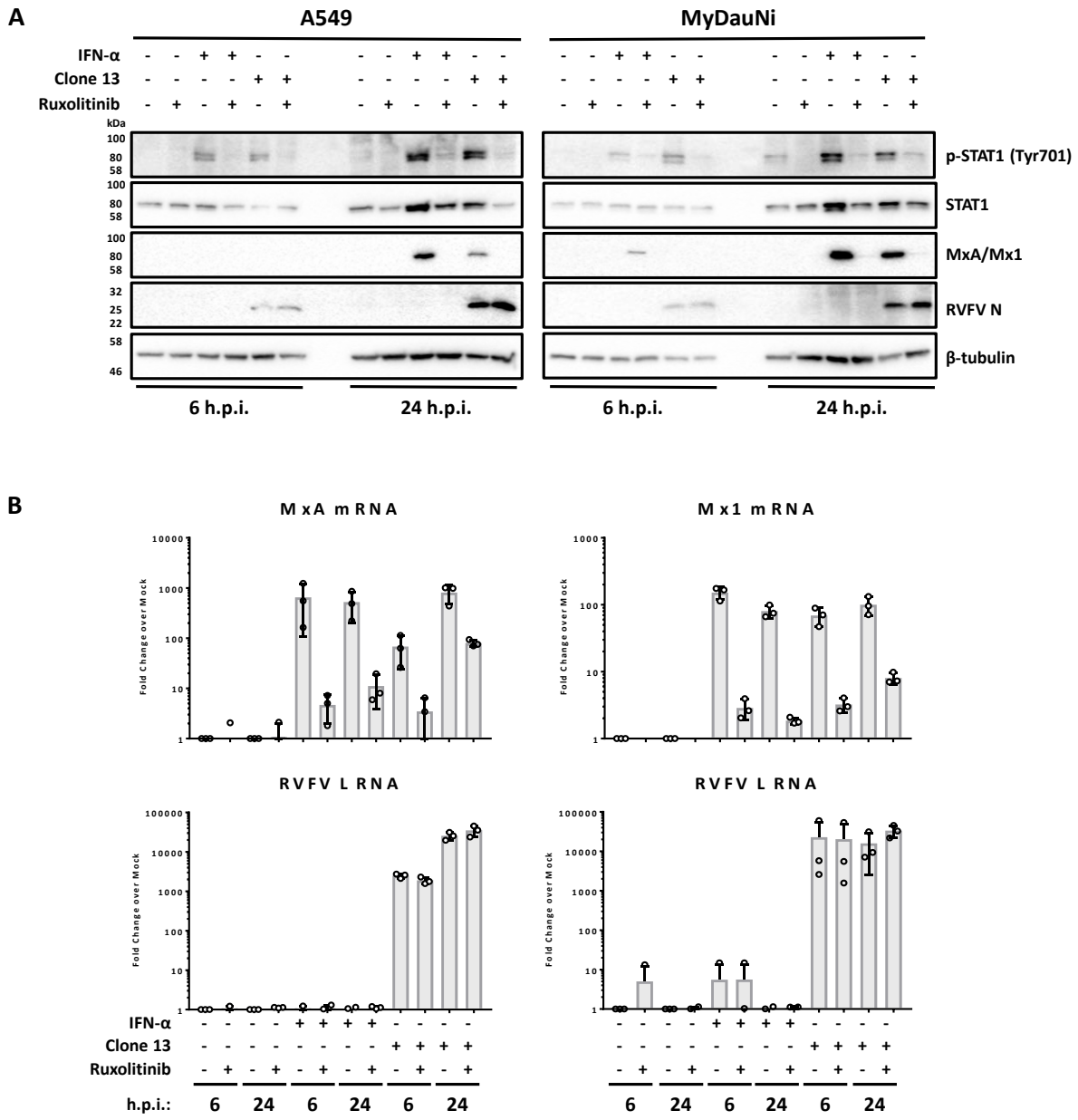

Figure S7, related to Figure 5. RT-qPCR confirmation of virus-only response genes - control experiments. Human A549 and *M. daubentonii* MyDauNi cells, treated or not with Ruxolitinib, were incubated with 1000 U/ml IFN-α or infected with Clone 13 (MOI 5) for 6 or 24 h, respectively. (A) Immunoblot analysis was performed with antibodies against the indicated antigens. Representative data from three independent experiments are shown. (B) RT-qPCR for MxA/Mx1 transcripts and the viral L segment, respectively. The graphs show the fold induction over mock, for the respective time point, with mean values and standard deviations from three independent replicates.

TRANSPARENT METHODS

KEY RESOURCES TABLE

REAGENT or RESOURCE	SOURCE	IDENTIFIER
Antibodies		
Rabbit polyclonal anti-phospho-Stat1 (Tyr701)	Cell Signaling	Cat# 9171
Mouse monoclonal anti-Stat1	BD Transduction Laboratories	Cat# 610185
Rabbit polyclonal anti- beta-tubulin	Abcam	Cat# ab6046
Mouse monoclonal anti-Mx (M143)	Georg Kochs, University of Freiburg, Germany	
Rabbit polyclonal anti-RVFV	Alejandro Brun, INIA, Madrid	
Virus Strains		
RVFVΔNSs::Renilla	Weber laboratory (Kuri et al., 2010)	N/A
Clone 13 (mutant RVFV strain)	Bouloy laboratory, Institute Pasteur, Paris (Billecocq et al., 2004)	N/A
Chemicals, Peptides, and Recombinant Proteins		
Pan-species IFN-α (B/D)	PBL Biomedical Laboratories	
Ruxolitinib	Selleckchem	Cat# S1378
Critical Commercial Assays		
Dual-Luciferase Reporter Assay System	Promega	Cat# E1960
RNeasy Plus Mini Kit (250)	Qiagen	Cat# 74106
PrimeScript RT Reagent Kit with gDNA Eraser	Takara	Cat# RR047A
SYBR Premix Ex Taq (Tli RNase H Plus) Kit	Takara	Cat# RR420
Premix Ex Taq (Probe qPCR) Kit	Takara	Cat# RR390
Experimental Models: Cell Lines		

A549 cells	Weber laboratory	N/A
MyDauNi/2c	Müller/Drosten laboratory	N/A
Ro6E-J cells cells	Müller/Drosten laboratory	N/A
Vero E6 cells	Weber laboratory	N/A
BHK cells	Weber laboratory	N/A
Oligonucleotides		
Human IFNB1	Qiagen	Cat# QT00203763
Human CCL4	Qiagen	Cat# QT01008070
Human CH25H	Qiagen	Cat# QT00202370
Human STEAP4	Qiagen	Cat# QT00081403
Human MxA	Qiagen	Cat# QT00090895
18S RNA	Qiagen	Cat# QT00199367
Primer for human IFNL2/3 RT-qPCR Forward: 5' GCCTCTGTCACCTTCAACCTC 3'	(Spann et al., 2004)	N/A
Primer for human IFNL2/3 RT-qPCR Reverse 5' GGAGGGTCAGACACACAGGT3'	(Spann et al., 2004)	N/A
Primer for *M. daubentonii* IFNB1 RT-qPCR Forward: 5' AAAGCAGCAATTCAGCCTGT 3'		
Primer for *M. daubentonii* IFNB1 RT-qPCR Reverse: 5' CTGCTGGAGCATCTCGTACA 3'		
Primer for *M. daubentonii* CCL4 RT-qPCR Forward: 5' TCTGCTCTCCAGTGCTCTCA 3'		
Primer for *M. daubentonii* CCL4 RT-qPCR Reverse: 5' AGATCTGTCTGCCCCTTTTG 3		
Primer for *M. daubentonii* IFNL3 RT-qPCR Forward: 5' CACATCCACTCCAAGCTTCA 3'		
Primer for *M. daubentonii* IFNL3 RT-qPCR Reverse: 5' TCAGCGACACATCTCAGGTC 3'		

Primer for *M. daubentonii* CH25H RT-qPCR Forward: 5' TCTTCCACACGCTCAACATC 3		
Primer for *M. daubentonii* CH25H RT-qPCR Reverse: 5' GGGGCGAAGTTGTAGTTGAA 3'		
Primer for *M. daubentonii* STEAP4 RT-qPCR Forward: 5' CCCAGAGTCCAATGCAGAGT 3'		
Primer for *M. daubentonii* STEAP4 RT-qPCR Reverse: 5' GTTGCAGGGGGTAGTTTTCA 3'		
Primer for *M. daubentonii* Mx1 RT-qPCR Forward: 5' CAGAGGGAGAGGGCTTTCTT 3		
Primer for *M. daubentonii* Mx1 RT-qPCR Reverse: 5' TCTGCTGGTTCTCCTTTATTTG 3'		
Primer for *M. daubentonii* 18S rRNA RT-qPCR Forward: 5' AAACGGCTACCACATCCAAG 3		
Primer for *M. daubentonii* 18S rRNA RT-qPCR Reverse: 5' CCTCCAATGGATCCTCGTTA 3'		
Primer for RVFV L segment RNA RT-qPCR	(Bird et al., 2007)	
Software and Algorithms		
Ensembl (Myoluc2.0, release 86)		
GraphPad Prism 7		
STAR (v2.5.2)	(Dobin and Gingeras, 2015)	
CLARK (v1.2.5)	(Ounit et al., 2015)	
Krona (v2.7)	(Ondov et al., 2011)	
blastx (v2.4.0+)		
Trinotate pipeline (v3.0.2)	https://trinotate.github.io/	
featureCounts(v1.5.0)	(Liao et al., 2014)	
ReportingTools package	(Huntley et al., 2013)	
Piano package	(Varemo et al., 2013)	

PCAGO web service	https://doi.org/10.1101/433078	
BinPacker (v1.1)	(Liu et al., 2016)	
IDBA-Tran (v1.1.1)	(Peng et al., 2013)	
SPAdes in single-cell and RNA modus (v3.10.1)	(Bankevich et al., 2012)	
SOAPdenovo-trans (v1.03)	(Xie et al., 2014)	
Trinity (v2.3.2)	(Grabherr et al., 2011)	
CD-HIT-EST (v4.6; -c 0.95)	(Fu et al., 2012)	
MAFFT (v7.402; L-INS-i parameter)	(Katoh and Standley, 2013)	
RAxML (v8.0.25)	(Stamatakis, 2014)	
Newick Utilities suite (v1.6)	(Junier and Zdobnov, 2010)	
Inkscape (v0.92.1)	https://inkscape.org	

CONTACT FOR REAGENT AND RESOURCE SHARING

Further information and requests for resources and reagents should be directed to and will be fulfilled by the Lead Contact, Friedemann Weber (friedemann.weber@vetmed.uni-giessen.de).

EXPERIMENTAL MODELS AND SUBJECT DETAILS

Cells, viruses, and reagents

Human lung A549 and the *M. daubentonii* kidney cell line MyDauNi/2c (Fuchs et al., 2017; Muller et al., 2012) were propagated in CCM-34 medium (4,5 g/L DMEM supplemented with 200 µM L-Alanine, 225 µM L-Aspartic acid, 933 µM Glycin, 510 µM L-Glutamic acid, 217 µM L-Proline, 184 µM Hypoxanthine, 0,1 mg/L Biotin, 44 mM NaHCO3, 10 % FBS, 10 U/L Penicillin, 10 µg/L Streptomycin and 292 µg/L L-glutamine. *R. aegytiacus* Ro6E-J cells (Jordan et al., 2009), human A549 cells, simian VeroE6 cells and hamster BHK cells were propagated in DMEM (Gibco/ Thermo Fisher Scientific) supplemented with 100 µM Glycine, 100 µM L-Alanine, 100 µM L-Asparagine, 100 µM L-Aspartic acid, 100 µM L-Glutamic Acid, 100 µM L-Proline, 100 µM L-Serine, 10 % FBS, 10 U/L Penicillin, 10 µg/L Streptomycin and 292 µg/L L-Glutamine. Recombinant Rift Valley fever virus mutant (RVFVΔNSs::Renilla)(Kuri et al., 2010) and the natural NSs-deficient mutant Clone 13 (Billecocq et al., 2004), were propagated on BHK cells and titrated on Vero E6 cells as described.

Assays for cellular IFN competence

To test for STAT1-dependent responses, cells where either treated with 1 µM of Ruxolitinib for 1 h, and/or 500 U/ml pan-species IFN-α (B/D) for 30 min, or left untreated. After lysis of cells, immunoblot analysis was performed with primary antibodies against phospho-Stat1, Stat1 (both 1:1000), and tubulin (1:2000).

To test for the ability to produce antiviral IFN in response to infection, cells were pretreated with 30 nM Ruxolitinib (1 h prior to infection) or 500 U/ml IFN-α (B/D) (16 h prior to infection), or left untreated. The cells were then infected with RVFVΔNSs::Renilla at a multiplicity of infection (MOI) of 1. Ruxolitinib and IFN were added also to the cell culture medium for the duration of the infection. At 48 h post-infection, cells were lysed and subjected to Renilla luciferase assays as described by the manufacturer (Promega Dual Luciferase kit) on a TriStar2 Multimode Reader LB 942 (Berthold).

Next-Generation Sequencing design and RNA-Seq

Total cellular RNA was isolated at 6 h and at 24 h post infection (1.200.000 cells per condition and time point), approved for their integrity using an Agilent 2100 Bioanalyzer, and subjected to RNA deep sequencing. For each total RNA sample cDNA libraries were prepared utilizing the Illumina Ribo-Zero rRNA Removal Kit for human/mouse/rat (hereafter rRNA-). Importantly, no polyA selection was applied. Overall, 18 rRNA- libraries were sequenced on six HiSeq 2500 lanes with 51 cycles resulting in 60-70 million strand-specific single-end reads per sample (Tab. S1). The complete experiment was performed in three independent, biological replicates. The raw read data was deposited in the GEO database under accession number GEO: GSE121301.

Data processing, quality control and mapping

Since no reference genome for *M. daubentonii* is publicly available, we downloaded the reference sequence and annotation of the closely related *M. lucifugus* from Ensembl (Myoluc2.0, release 86). Reference sequences for the L, M, and S segment of RVFV were downloaded from the NCBI under RefSeq accessions NC014397.1, NC014395.1, and NC014396.1. The genomic sequence of *M. lucifugus* and the RVFV sequences were concatenated for mapping the RNA-Seq-derived short reads. Prior to mapping, all samples were quality checked with FastQC and quality trimmed with a Q20 threshold and a window size of length 4 using Prinseq (v0.20.3) (Schmieder and Edwards, 2011). Reads shorter than 15 nt were discarded from the analysis. We used SortMeRNA (v2.1) (Kopylova et al., 2012) to detect and remove ribosomal RNAs, possibly still remaining after the ribosomal depletion step during cDNA library preparation. The quality-controlled and rRNA-depleted reads were mapped to the concatenated reference genomes of *M. lucifugus* and RVFV using STAR (v2.5.2) (Dobin and Gingeras, 2015) with an adjusted --outFilterScoreMinOverLread and --outFilterMatchNminOverLread of 0.4.

Read classification and Krona visualization

To check for possible contaminations in the RNA and the amount of viral reads in each sample, we used CLARK (v1.2.5) (Ounit et al., 2015) to classify the quality-checked reads against the NCBI RefSeq databases for viruses, bacteria, fungi, and human. We added the Ensembl *M. lucifugus* genome as a custom database and visualized the classification results of each sample with Krona (v2.7) (Ondov et al., 2011).

Extension of the *M. lucifugus* annotation

We used blastx (v2.4.0+) against the Uniprot/SwissProt database created with the Trinotate pipeline (v3.0.2; https://trinotate.github.io/) to extend the Ensembl gene annotation of *M. lucifugus*. All blast hits that were considered as true positive hits had to meet an E-value threshold of 10^{-4}, a sequence identity of at least 50% and an alignment length of at least 50%. If multiple hits for one sequence passed our filter settings, we selected the one with the best E-value. Based on this approach, we were able to assign a gene name and function to additional 4,844 sequences out of 7,101 CDS without a functional description in the Ensembl annotation for *M. lucifugus*. Additional homologous gene annotations were marked with a _<SPECIES> tag in the electronic supplement to distinguish between the original Ensembl annotation and our extension.

Based on our strand-specific RNA-Seq data and with the help of our *de novo* assembly, we found various IFN genes to be annotated on the wrong strand in the Ensembl annotation of *M. lucifugus*. Therefore, these genes got initially zero read counts when estimating expression values with featureCounts (v1.5.0) (Liao et al., 2014). To also take these genes into consideration, we adjusted the Ensembl annotation and changed the strand from '+' to '-' for the following gene IDs: ENSMLUG00000026947 (IFNA5_HUMAN), ENSMLUG00000027734, ENSMLUG00000023736 (IFNW2_HORSE), ENSMLUG00000027612, ENSMLUG00000028931 (IFNW2_HORSE), ENSMLUG00000024850, ENSMLUG00000027376. Moreover, IRF7 was before not annotated at all in the *M. lucifugus* genome and had to be manually corrected. We calculated the position of IRF7 in the *M. lucifugus* genome based on our mapped reads and NCBI blast searches to finally add its annotation on contig

AAPE02063415:16558-16759 on the minus strand. In addition, we identified ENSMLUG00000025338 as being ISG15.

RNA quantification, normalization and differential gene expression

We used featureCounts to quantify the mapped reads based on our extended and corrected Ensembl annotation (originally release 86) of *M. lucifugus* comprising 25,849 genes (19,728 coding for proteins). Reads were counted strand-specific on exon level and accumulated per gene ID to obtain one count per gene. Only uniquely mapped reads were used in the differential gene expression analysis and further evaluations.

The read counts were passed to DESeq2 (v1.16.1) (Love et al., 2014) to call significantly (adjusted $p \leq 0.05$) differentially expressed genes and to calculate fold changes between the different time points and conditions. To reduce the amount of low expressed genes and false positive hits, the DESeq2 results were additionally filtered by calculating TPM (transcripts per million) values for each gene and each sample as:

$$TPM_i = \frac{c_i}{l_i} \times \left(\frac{1}{\sum_{j \in N} \frac{c_j}{l_j}} \right) \times 10^6$$

where c_i is the raw read count of gene i, l_i is the cumulative exon length of gene i and N is the number of all genes in the given annotation. For each gene, we calculated six mean TPM values (TPM_M), based on the three biological replicates corresponding to the mock, IFN and Clone 13-infected samples at the two time points. If a protein-coding gene showed a $TPM_M > 1$ in at least one of the six conditions, it was considered as expressed and used for further analyses. Genes that did not show a $TPM_M > 1$ in at least one condition were marked and discarded from further analyses.

We used various R packages for visualization and data assessment, comprising extended functionalities of the DESeq2 package such as principal component analyses, gene expression scatter plots and heat maps. We used the ReportingTools package (Huntley et al., 2013) to generate interactive web pages of significantly differential expressed genes and to build expression box plots for all genes and samples. GO term enrichment and visualization of the most significant regulated gene sets was performed with the Piano package (Varemo et al., 2013).

Principal component analyses were performed using the PCAGO web service (https://doi.org/10.1101/433078). As input, unique read counts of all 18 samples were used and DESeq2-normalized and rlog-transformed with the build in functionalities of the web service. Genes with zero or constant read counts were removed prior PCA and the top 500 variant genes were finally used for the transformation shown in Fig.3. Supplemental 2d- and 3d-PCA movies were generated starting with the top 10 variant genes and adding step-wise 10 genes until reaching all 21,791 genes without zero or constant read count.

De novo transcriptome assembly

Based on a comparison of current *de novo* assembly tools for short-read RNA-Seq data (Holzer and Marz, 2019), we used SPAdes in single-cell and RNA modus (v3.10.1) (Bankevich et al., 2012), SOAPdenovo-trans (v1.03) (Xie et al., 2014), and Trinity (v2.3.2) (Grabherr et al., 2011) to build a comprehensive transcriptome assembly for *M. daubentonii*. As input, the quality-checked reads of all 18 samples were used. All assembly tools were executed with default parameters and, if possible, in strand-specific mode. The resulting contigs of all tools were merged with CD-HIT-EST (v4.6; -c 0.95) (Fu et al., 2012) and the final assembly was used for homology searches and to confirm observations obtained from the *M. lucifugus*-based genome analyses. To investigate also (*de novo*) transcripts and isoforms differing between the conditions, triplicate samples were merged and assembled with Trinity only.

Phylogenetic analysis of BST2

We downloaded twelve CDS of mammalian BST2 genes for *Pteropus vampyrus* (ENSPVAG00000007879), *Rousettus aegyptiacus* (NW_015494646), *Sus scrofa* (ENSSSCG00000033453), *Rattus norvegicus* (ENSRNOG00000059900), *Ovis aries* (ENSOARG00000025182, ENSOARG00000016787), *Gorilla gorilla* (ENSGGOG00000015278), *Canis familiaris* (ENSCAFG00000031353), *Bos taurus* (ENSBTAG00000008021), *Homo sapiens* (ENSG00000130303), *Mus musculus* (ENSMUSG00000046718), and *Pan troglodytes* (ENSPTRG00000010672) from Ensembl (release 93) and NCBI. We expanded this list by four potential BST2 paralogous genes, identified with the help of our extended annotation, from the *M. lucifugus* genome: ENSMLUG00000023562, ENSMLUG00000023691, ENSMLUG00000026989, and ENSMLUG00000029243. Furthermore, we extracted three potential BST2 transcripts from the *de novo* transcriptome assembly of *M. daubentonii*. Interestingly, we were only able to identify three BST2-like transcripts with a differing sequence in the assembly. Overall, we aligned 18 BST2-coding sequences with MAFFT (Katoh and Standley, 2013) (v7.402; L-INS-i parameter) and calculated a phylogenetic tree with RAxML (v8.0.25) (Stamatakis, 2014) using 1000 bootstraps, the GTRGAMMA model, and the primate BST2 CDS as outgroups. We used Inkscape (v0.92.1; available from https://inkscape.org) to finalize the tree and other figures for publication.

Verification of uniquely virus-regulated genes

A549 cells and MyDauNi cells (5×10E4 per well) where seeded in 24-well plates, grown overnight, and then either infected with RVFV Clone 13 (MOI 5), incubated with 1000 U/ml IFN-α (B/D), or left untreated, all with or without 1 µM Ruxolitinib as indicated. Cells were kept under the respective conditions and total RNA isolated 6 and 24 h post-infection using the RNeasy Mini Kit (Qiagen). A total of 100 ng RNA/sample was used for cDNA synthesis using the PrimeScript RT Reagent Kit with gDNA Eraser (Takara) according to manufacturer's instructions. The kit included a step for removal of possible contamination by genomic DNA. RT-qPCR was performed using the SYBR Premix Ex Taq (Tli RNase H Plus) and the Premix Ex Taq (Probe qPCR) Kit (Takara) on a StepOnePlus Real-Time PCR machine (Applied Biosystems). For primer sequences, see Key Resources Table. All data obtained were normalised against the 18S RNA signal using the ddCT method.

To confirm IFN competence and Ruxolitinib efficacy, cells infected and treated as indicated above were analysed by immunoblot with primary antibodies against phospho-Stat1, Stat1 and tubulin as indicated, and against Mx1 and RVFV N at 1:1000 and 1:2000, respectively.

Electronic Supplement

The electronic supplement can be found at https://www.rna.uni-jena.de/supplements/mda/ comprising additional information about the RNA-Seq quality and read pre-processing, mapping statistics, PCA plots and videos, a read classification with Clark, GO term enrichment, full tables (including Excel) and further statistics for all differential expressed genes of each pairwise comparison, and coverage plots of the viral reads mapping to the S, L, and M segment of the RVFV reference genome. We used the DESeq2 results and the visualizations of the ReportingTools (Huntley et al., 2013) package to build an interactive gene observer (IGO), containing 1,448 genes that have a significant hit (q-value < 0.05) and an absolute fold change > 1 in at least one of the four comparisons Mock:IFN 6 h, Mock:IFN 24 h, Mock:Clone13 6 h, and Mock:Clone13 24 h. Our online tool is available at https://www.rna.uni-jena.de/supplements/mda/report.html and can be easily used to search for gene names and Ensembl gene IDs of the *M. lucifugus* reference genome used.

For full reproducibility of our study, we also uploaded the raw read data in the GEO database under accession number GEO: GSE121301. Moreover, all intermediate files such as the quality-trimmed and rRNA-cleaned reads of all 18 samples, mappings, the extended genome annotation and raw read counts to the Open Science Framework under https://doi.org/10.17605/OSF.IO/X9KAD.

REFERENCES

Bankevich, A., Nurk, S., Antipov, D., Gurevich, A.A., Dvorkin, M., Kulikov, A.S., Lesin, V.M., Nikolenko, S.I., Pham, S., Prjibelski, A.D*., et al.* (2012). SPAdes: a new genome assembly algorithm and its applications to single-cell sequencing. J Comput Biol *19*, 455-477.

Billecocq, A., Spiegel, M., Vialat, P., Kohl, A., Weber, F., Bouloy, M., and Haller, O. (2004). NSs protein of Rift Valley fever virus blocks interferon production by inhibiting host gene transcription. Journal of virology *78*, 9798-9806.

Bird, B.H., Bawiec, D.A., Ksiazek, T.G., Shoemaker, T.R., and Nichol, S.T. (2007). Highly sensitive and broadly reactive quantitative reverse transcription-PCR assay for high-throughput detection of Rift Valley fever virus. J Clin Microbiol *45*, 3506-3513.

Dobin, A., and Gingeras, T.R. (2015). Mapping RNA-seq Reads with STAR. Curr Protoc Bioinformatics *51*, 11 14 11-19.

Fu, L., Niu, B., Zhu, Z., Wu, S., and Li, W. (2012). CD-HIT: accelerated for clustering the next-generation sequencing data. Bioinformatics *28*, 3150-3152.

Fuchs, J., Holzer, M., Schilling, M., Patzina, C., Schoen, A., Hoenen, T., Zimmer, G., Marz, M., Weber, F., Muller, M.A*., et al.* (2017). Evolution and Antiviral Specificities of Interferon-Induced Mx Proteins of Bats against Ebola, Influenza, and Other RNA Viruses. Journal of virology *91*.

Grabherr, M.G., Haas, B.J., Yassour, M., Levin, J.Z., Thompson, D.A., Amit, I., Adiconis, X., Fan, L., Raychowdhury, R., Zeng, Q.D*., et al.* (2011). Full-length transcriptome assembly from RNA-Seq data without a reference genome. Nat Biotechnol *29*, 644-U130.

Holzer, M., and Marz, M. (2019). De novo transcriptome assembly: A comprehensive cross-species comparison of short-read RNA-Seq assemblers. Gigascience *8*.

Huntley, M.A., Larson, J.L., Chaivorapol, C., Becker, G., Lawrence, M., Hackney, J.A., and Kaminker, J.S. (2013). ReportingTools: an automated result processing and presentation toolkit for high-throughput genomic analyses. Bioinformatics *29*, 3220-3221.

Jordan, I., Horn, D., Oehmke, S., Leendertz, F.H., and Sandig, V. (2009). Cell lines from the Egyptian fruit bat are permissive for modified vaccinia Ankara. Virus research *145*, 54-62.

Junier, T., and Zdobnov, E.M. (2010). The Newick utilities: high-throughput phylogenetic tree processing in the UNIX shell. Bioinformatics *26*, 1669-1670.

Katoh, K., and Standley, D.M. (2013). MAFFT multiple sequence alignment software version 7: improvements in performance and usability. Mol Biol Evol *30*, 772-780.

Kopylova, E., Noe, L., and Touzet, H. (2012). SortMeRNA: fast and accurate filtering of ribosomal RNAs in metatranscriptomic data. Bioinformatics *28*, 3211-3217.

Kuri, T., Habjan, M., Penski, N., and Weber, F. (2010). Species-independent bioassay for sensitive quantification of antiviral type I interferons. Virology journal *7*, 50.

Liao, Y., Smyth, G.K., and Shi, W. (2014). featureCounts: an efficient general purpose program for assigning sequence reads to genomic features. Bioinformatics *30*, 923-930.

Liu, J., Li, G., Chang, Z., Yu, T., Liu, B., McMullen, R., Chen, P., and Huang, X. (2016). BinPacker: Packing-Based De Novo Transcriptome Assembly from RNA-seq Data. PLoS Comput Biol *12*, e1004772.

Love, M.I., Huber, W., and Anders, S. (2014). Moderated estimation of fold change and dispersion for RNA-seq data with DESeq2. Genome biology *15*, 550.

Muller, M.A., Raj, V.S., Muth, D., Meyer, B., Kallies, S., Smits, S.L., Wollny, R., Bestebroer, T.M., Specht, S., Suliman, T*., et al.* (2012). Human Coronavirus EMC Does Not Require the SARS-Coronavirus Receptor and Maintains Broad Replicative Capability in Mammalian Cell Lines. Mbio *3*.

Ondov, B.D., Bergman, N.H., and Phillippy, A.M. (2011). Interactive metagenomic visualization in a Web browser. BMC Bioinformatics *12*, 385.

Ounit, R., Wanamaker, S., Close, T.J., and Lonardi, S. (2015). CLARK: fast and accurate classification of metagenomic and genomic sequences using discriminative k-mers. BMC genomics *16*.

Peng, Y., Leung, H.C., Yiu, S.M., Lv, M.J., Zhu, X.G., and Chin, F.Y. (2013). IDBA-tran: a more robust de novo de Bruijn graph assembler for transcriptomes with uneven expression levels. Bioinformatics *29*, i326-334.
Schmieder, R., and Edwards, R. (2011). Quality control and preprocessing of metagenomic datasets. Bioinformatics *27*, 863-864.
Spann, K.M., Tran, K.C., Chi, B., Rabin, R.L., and Collins, P.L. (2004). Suppression of the induction of alpha, beta, and gamma interferons by the NS1 and NS2 proteins of human respiratory syncytial virus in human epithelial cells and macrophages. Journal of virology *78*, 4363-4369.
Stamatakis, A. (2014). RAxML version 8: a tool for phylogenetic analysis and post-analysis of large phylogenies. Bioinformatics *30*, 1312-1313.
Varemo, L., Nielsen, J., and Nookaew, I. (2013). Enriching the gene set analysis of genome-wide data by incorporating directionality of gene expression and combining statistical hypotheses and methods. Nucleic acids research *41*, 4378-4391.
Xie, Y., Wu, G., Tang, J., Luo, R., Patterson, J., Liu, S., Huang, W., He, G., Gu, S., Li, S.*, et al.* (2014). SOAPdenovo-Trans: de novo transcriptome assembly with short RNA-Seq reads. Bioinformatics *30*, 1660-1666.